Elaborate ligand-based modeling and subsequent synthetic exploration unveil new nanomolar Ca^{2+}/calmodulin-dependent protein kinase II inhibitory leads

Rand Shahin, Mutasem O. Taha *

Drug Discovery Unit, Department of Pharmaceutical Sciences, Faculty of Pharmacy, University of Jordan, Amman, Jordan

A B S T R A C T

Ca^{2+}/calmodulin-dependent protein kinase II (CaMKII) has been recently implicated in cardiovascular diseases and hypertension prompting several attempts to discover and optimize new CaMKIIδ inhibitors. Towards this end we explored the pharmacophoric space of 88 CaMKIIδ inhibitors using nine diverse sets of inhibitors to identify high quality pharmacophores. Subsequently, genetic algorithm and multiple linear regression analysis were employed to select an optimal combination of pharmacophoric models and 2D physicochemical descriptors capable of accessing self-consistent quantitative structure–activity relationship (QSAR) of optimal predictive potential ($r^2_{72} = 0.70$, $F = 18.19$, $r^2_{LOO} = 0.71$, r^2_{PRESS} against 16 external test inhibitors = 0.60). Three orthogonal pharmacophores emerged in the QSAR equation suggesting the existence of at least three binding modes accessible to ligands within CaMKIIδ binding pocket. Receiver operating characteristic (ROC) curves analysis established the validity of QSAR-selected pharmacophores. We employed the pharmacophoric models and associated QSAR equation to screen the national cancer institute (NCI) list of compounds. In silico screening identified nanomolar and low micromolar inhibitors. The most potent hits exhibited IC$_{50}$ values of 20 and 82 nM. The best pharmacophoric model (Hypo8/31) was employed to guide the synthesis of novel triazine-based CaMKIIδ inhibitors, of which the most potent illustrated an IC$_{50}$ value of 154 nM against CaMKIIδ.

© 2011 Elsevier Ltd. All rights reserved.

1. Introduction

1.1. Ca^{2+}/calmodulin-dependent protein kinase II

Ca^{2+}/calmodulin-dependent protein kinase II (CaMKII), which is a member of Ca^{2+}/calmodulin-dependent protein kinases (three subtypes I, II and IV), is a multifunctional serine/threonine kinase that acts as an ubiquitous mediator of Ca^{2+}-linked signaling. It phosphorylates a wide range of substrates involved in regulating Ca^{2+} mediated alterations in cellular function.[1]

There are four CaMKII isoforms (α, β, γ, and δ) distributed in various tissues: CaMKIIα and β are found primarily in the brain, while CaMKIIδ is found in the heart.[2] CaMKIIδ is involved in diverse myocardial roles including regulation of excitation, contraction, transcription, and apoptosis. Therefore, it represents an attractive target for therapeutic intervention in cardiovascular diseases.[2,3,46–49]

Like other Ca^{2+}/calmodulin-dependent protein kinases, CaMKIIδ is regulated by calmodulin (CaM), which is an ubiquitous Ca^{2+} sensor protein that activates substrates proteins and enzymes in a Ca^{2+}-dependent manner.[6] CaM binding to CaMKIIδ induces conformational changes in CaMKIIδ that relieves autoinhibition and allows full enzyme activity.[3,4]

The validity of CaMKII as a target for therapeutic intervention in cardiovascular diseases was established by emerging clinical trials employing potent CaMKII inhibitors: KN-62, KN-93 and the natural CaMKII inhibitor staurosporine.[1]

However, despite their high cellular activity and clinical progression, CaMKIIδ inhibitors suffer from several limitations, such as, poor cellular permeability, general toxicity, and specificity.[1] These issues have led to significant efforts to identify novel small molecular inhibitors of CaMKIIδ.[1,5,6,20,21]

Despite the recent availability of satisfactory high resolution crystallographic structure for CaMKIIδ (PDB code: 2vn9, resolution 2.3 Å), most related discovery projects were confined to high throughput screening[42] and homology modeling.[1]

The continued interest in designing new CaMKIIδ inhibitors combined with the lack of adequate ligand-based computer-aided drug discovery efforts prompted us to explore the possibility of developing ligand-based three-dimensional (3D) pharmacophore(s) integrated within self-consistent QSAR model. The pharmacophore model(s) can be used as 3D search queries to discover new CaMKIIδ inhibitory scaffolds, while the QSAR model can be used to predict the bioactivities of captured hits and to prioritize them for in vitro testing. We previously reported the use of
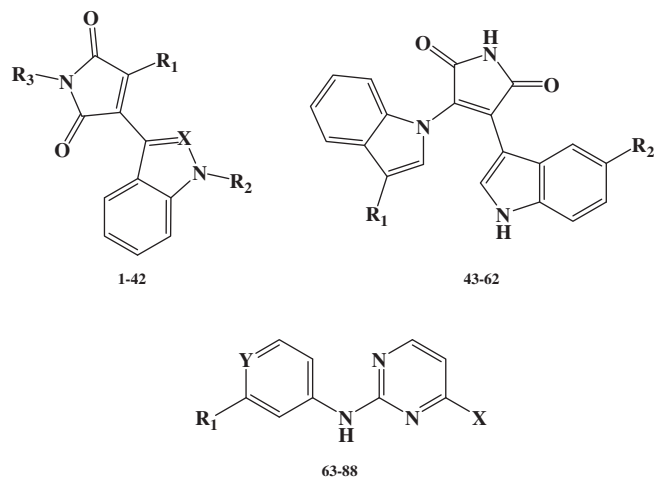
Figure 1. The chemical scaffolds of training compounds, the detailed structures are as in Table A under Supplementary data.

Table 1
The cross correlation coefficients (r^2) between the successful pharmacophoric hypotheses in Eq. 1[a,b,c]

	Hypo8/31	Hypo 9/47
Hypo 9/47	0.107	
Hypo 7/39	0.288	0.027

[a] Regression values were calculated by cross-correlating the fit values of training compounds (used in QSAR modeling) determined for each corresponding pharmacophore (as in Eq. (D) in Supplementary data).
[b] Descriptive statistics of pharmacophore fit values used in calculating the correlation matrix are shown in Table E2 under Supplementary data.
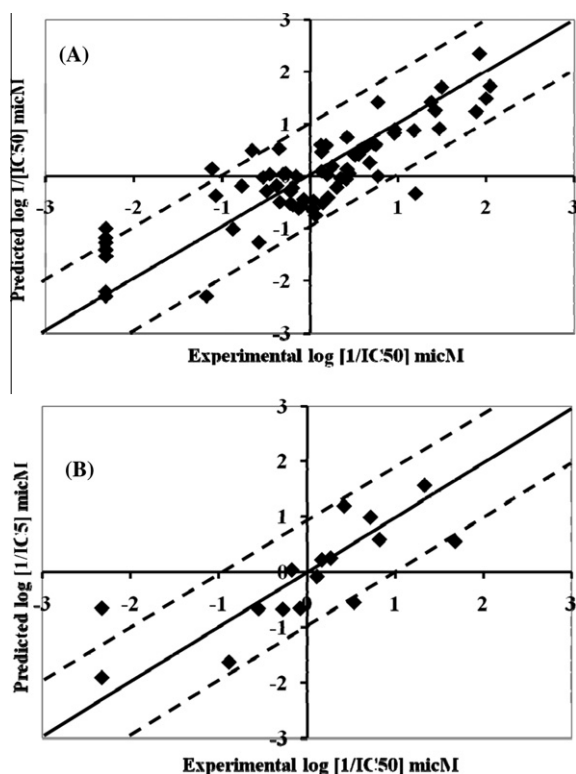[c] Correlation without uncertainty parameter.

Figure 2. Experimental versus (A) fitted (72 compounds, $r^2_{\mathrm{LOO}} = 0.71$), and (B) predicted (16 compounds, $r^2_{\mathrm{PRESS}} = 0.60$) bioactivities calculated from the best QSAR model Eq. 1. The solid lines are the regression lines for the fitted and predicted bioactivities of training and test compounds, respectively, whereas the dotted lines indicate 1.0 log point error margins.

this innovative approach towards the discovery of new inhibitory leads against glycogen synthase kinase-3β,[7] bacterial MurF,[8] protein tyrosine phosphatase,[9] DPP IV,[10] hormone sensitive lipase,[11] β-secretase,[12] influenza neuraminidase,[13] cholesteryl ester transfer protein,[14] cycline dependent kinase,[15] heat shock protein,[16] estrogen receptor β,[17] β-D-glucosidase,[18] and β-D-galactosidase.[19]

We employed the CATALYST-HYPOGEN module of the software package Discovery Studio[23] to construct numerous plausible binding hypotheses for a diverse list of CaMKIIδ inhibitors.[5,6,20,21] Subsequently, genetic function algorithm (GFA) and multiple linear regression (MLR) analyses were employed to search for an optimal QSAR that combine high-quality binding pharmacophores with other molecular descriptors and capable of explaining bioactivity variation across a collection of diverse CaMKIIδ inhibitors. The optimal pharmacophores were subsequently used as 3D search
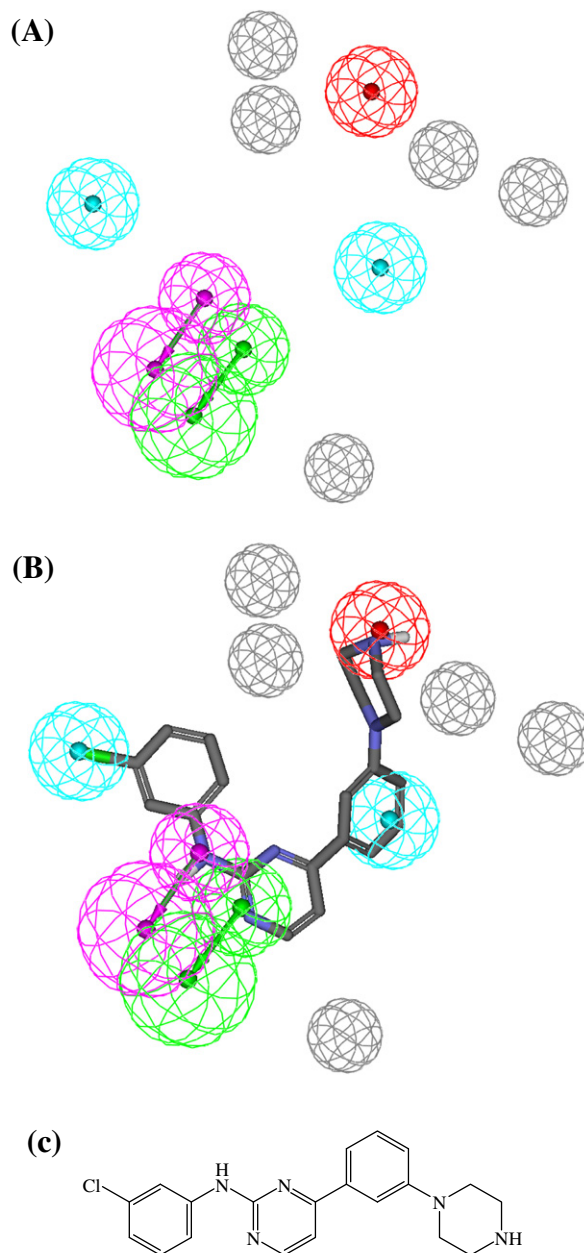

Figure 3. (A) Pharmacophoric features of Hypo8/31: HBD as pink vectored spheres, HBA as green vectored spheres, Hbic as blue spheres, PosIon as red spheres, Exclusion volumes as grey spheres, (B) Hypo8/31 fitted against training compound **85** (IC$_{50}$ = 0.009 μM, Table A under Supplementary data), (C) chemical structure of **85**.

queries to screen the national cancer institute (NCI) list of compounds for new CaMKIIδ inhibitory leads that were tested in vitro. The resulting active hits and pharmacophores were used to guide synthesis of novel nanomolar triazine-based CaMKII inhibitors.

2. Results and discussion

2.1. Ligand-based modelling

CATALYST-HYPOGEN models drug–receptor interaction using information derived only from the ligand structure. It enables automatic pharmacophore construction by using a collection of molecules with activities ranging over a number of orders of magnitude. It identifies a 3D array of a maximum of five chemical features common to active training molecules, which provides a relative alignment for each input molecule consistent with their binding to a proposed common receptor site. The chemical features considered can be hydrogen bond donors and acceptors (HBDs and

HBAs), aliphatic and aromatic hydrophobes (Hbic), positive and negative ionizable (PosIon and NegIon) groups and aromatic planes (RingArom). The conformational flexibility of training ligands is modeled by creating multiple conformers, judiciously prepared to emphasize representative coverage over a specified energy range.[22,24] CATALYST pharmacophores have been used as 3D queries for database searching and in 3D.[7–19]

Different pharmacophoric hypotheses were generated for a series of CaMKIIδ inhibitors: A total of 88 compounds (Fig. 1 and Table A under Supplementary data).[5,6,20,21] Nine training subsets were selected from the collection (Table B under Supplementary data) and were used in pharmacophore exploration. Each subset consisted of inhibitors of wide structural diversity that appear to follow certain 3D structure–activity relationship (SAR) rule. The biological activity in the training subsets spanned from 3.5 to 4.0 orders of magnitude.[5,6,20,21] Overall, we implemented a pharmacophore exploration approach similar to our previous ligand-based lead discovery projects.[9–19]

Figure 4. (A) and (B) show pharmacophoric features of Hypo9/47 without and with stericrefinement, respectively. HBD as pink vectored spheres, Hbic as blue spheres, RingArom as vectored orange spheres, Exclusion volumes as grey spheres, (C) and (D) Hypo9/47 mapped against training compound **85** (IC$_{50}$ = 0.009 μM, Table A under Supplementary data) without and with stericrefinement, respectively, (E) chemical structure of **85**.

2.1.1. Data mining and conformational coverage

The literature was surveyed to collect many reported structurally diverse CaMKIIδ inhibitors (**1–88**, see Table A under Supplementary data and Fig. 1).[5,6,20,21] The 2D structures of the inhibitors were imported into CATALYST and converted automatically into 3D single conformer representations. The structures were used as starting points for conformational analyses and in the determination of various molecular descriptors for QSAR modeling.

The conformational space of each inhibitor was extensively sampled utilizing the poling algorithm employed within the CONFIRM module of CATALYST.[22] Conformational coverage was performed employing the 'Best' module to ensure extensive sampling of conformational space. Pharmacophore generation and pharmacophore-based search procedures are known for their sensitivity to inadequate conformational sampling within the training compounds prompting our extensive conformational sampling.[24]

2.1.2. Exploration of CaMKIIδ pharmacophoric space

The fact that we have an informative list of 88 CaMKIIδ inhibitors of evenly spread bioactivities over 3.5 orders of magnitude, prompted us to employ CATALYST-HYPOGEN to identify possible pharmacophoric binding modes assumed by CaMKδII inhibitors.[5,6,20,21]

HYPOGEN implements an optimization algorithm that evaluates large number of potential binding models for a particular target through fine perturbations to hypotheses that survived the constructive and subtractive phases of the modeling algorithm (see Sections 4.1.4 in Experimental and SM-1 in Supplementary data).[25] The extent of the evaluated pharmacophoric space is reflected by the configuration (Config.) cost calculated for each modeling run. It is generally recommended that the Config. cost of any HYPOGEN run not to exceed 17 (corresponding to 2^{17} hypotheses to be assessed by CATALYST) to guarantee thorough analysis of all models.[26] The size of the investigated pharmacophoric space is a function of training compounds, selected input chemical features and other CATALYST control parameters.[26]

Restricting the extent of explored pharmacophoric space should improve the efficiency of optimization via allowing effective evaluation of limited number of pharmacophoric models. On the other hand, rigorous restrictions imposed on the pharmacophoric space might reduce the possibility of discovering optimal pharmacophoric hypotheses, as they might occur outside the 'boundaries' of the pharmacophoric space.

Therefore, we decided to explore the pharmacophoric space of CaMKIIδ inhibitors under reasonably imposed 'boundaries' through 68 HYPOGEN automatic runs and employing nine carefully selected training subsets: subsets **I–IX** in Table B under Supplementary data. The training compounds in these subsets were selected in such away to guarantee maximal 3D diversity and continuous bioactivity spread over more than 3.5 logarithmic cycles.
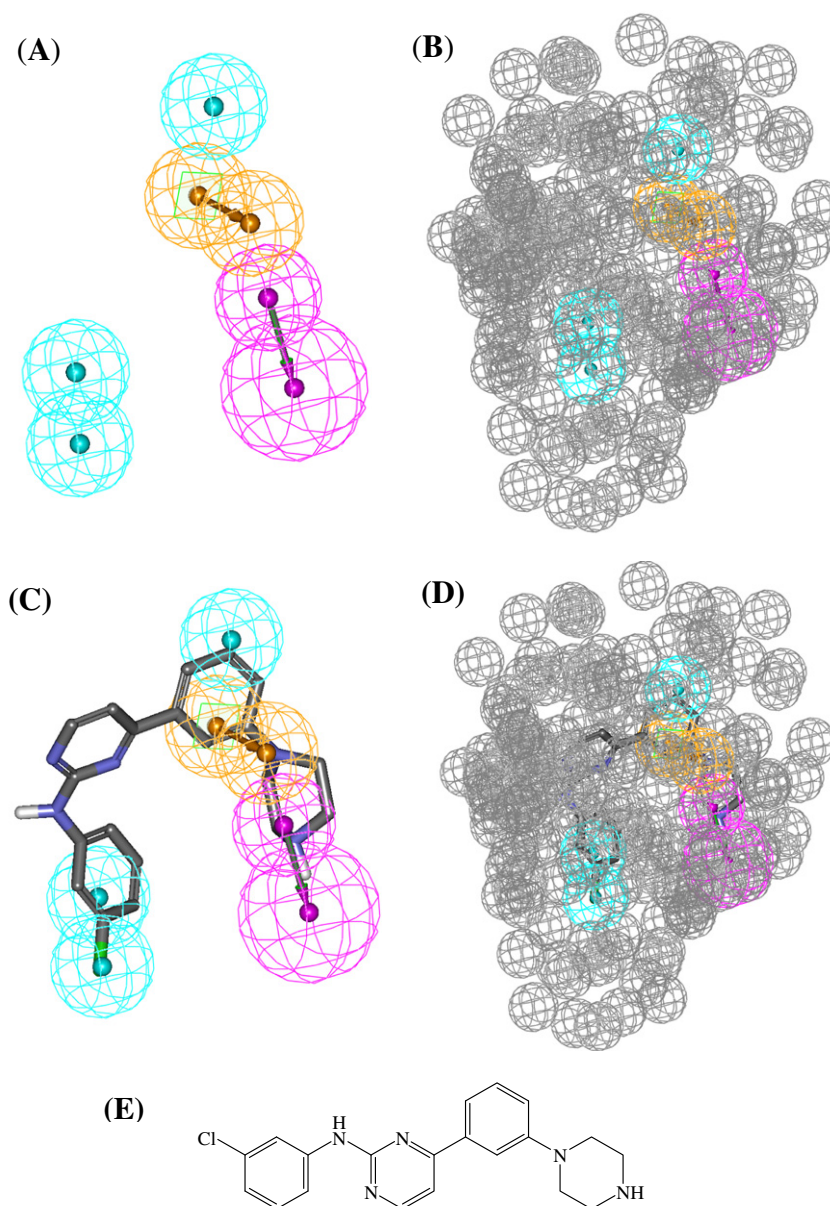

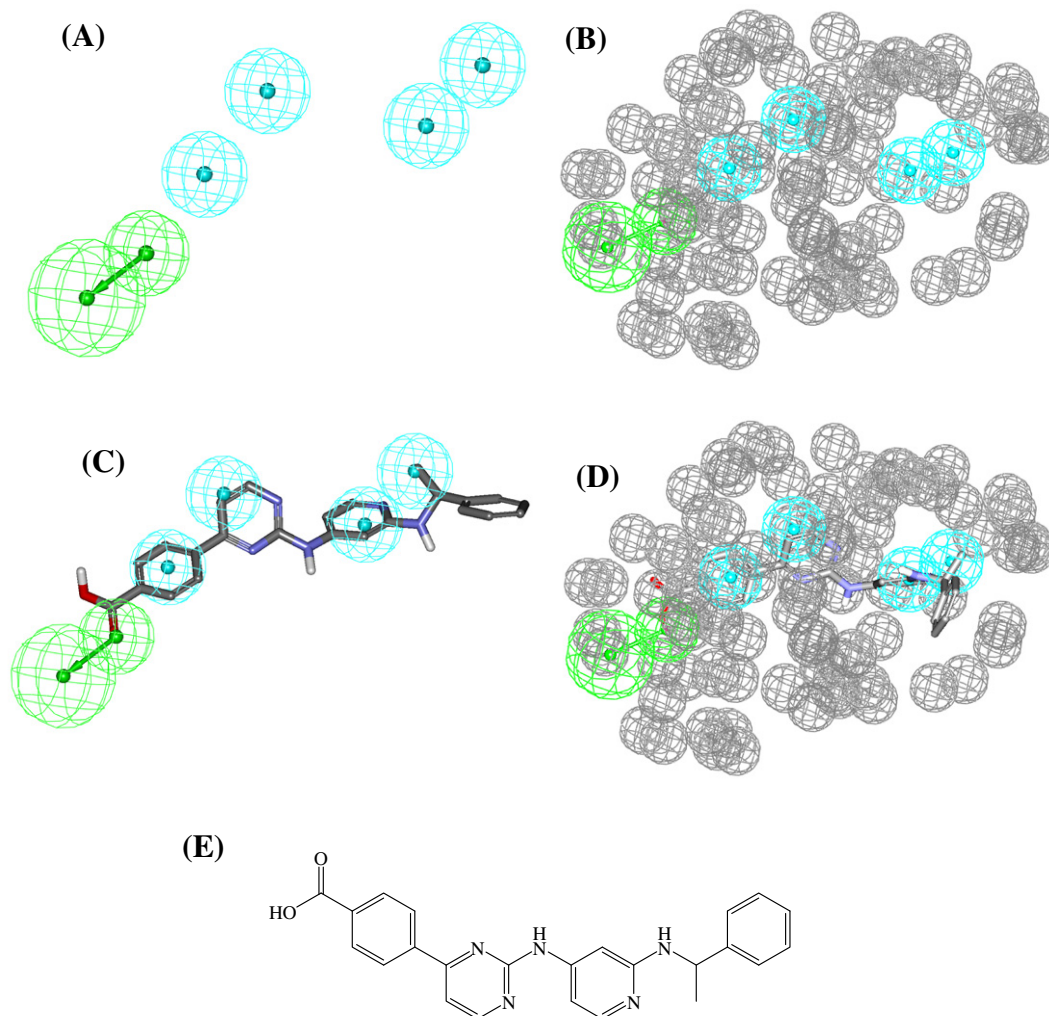**Figure 5.** (A) and (B) show pharmacophoric features of Hypo7/39 without and with steric-refinement, respectively. HBA as green vectored spheres, Hbic as blue spheres, exclusion volumes as grey spheres, (C) and (D) Hypo7/39 mapped against training compound **68** (IC$_{50}$ = 0.21 μM, Table A under Supplementary data) without and with steric-refinement, respectively, (E) chemical structure of **68**.

We gave special emphasis to the 3D diversity of the most active compounds in each training subset (Table B under Supplementary data) because of their significant influence on the extent of the evaluated pharmacophoric space during the constructive phase of HYPOGEN algorithm (see Section 4.1.4 Pharmacophoric Hypotheses Generation in Experimental and SM-1 under Supplementary data).[25]

Guided by our rationally restricted pharmacophoric exploration concept, we restricted the software to explore pharmacophoric models incorporating from zero to one PosIon or NegIon features, from zero to three HBA, Hbic, or RingArom features instead of the default range of zero to five, as shown in Table C under Supplementary data. Furthermore, we instructed HYPOGEN to explore only 4- and 5-featured pharmacophores, that is, ignore models of lesser number of features in order to further narrow the investigated pharmacophoric space and to represent the feature-rich nature of known CaMKIIδ ligands (as shown in Table C under Supplementary data).

In each run, the resulting binding hypotheses were automatically ranked according to their corresponding 'total cost' value, which is defined as the sum of error cost, weight cost and configuration cost (see Section 4.1.5 Assessment of the Generated Hypotheses in Experimental and Section SM-2 under Supplementary data).[22,25–29] Error cost provides the highest contribution to total cost and it is directly related to the capacity of the particular pharmacophore as 3D-QSAR model, that is, in correlating the molecular structures to the corresponding biological responses.[22,25–29] HYPOGEN also calculates the cost of the null hypothesis, which presumes that there is no relationship in the data and that experimental activities are normally distributed about their mean. Accordingly, the greater the difference from the null hypothesis cost (residual cost, Table 1) the more likely that

Table 3
ROC curve analysis criteria for QSAR-selected pharmacophores and their sterically-refined versions

Pharmacophore model	ROC[a]–AUC[b]	ACC[c]	SPC[d]	TPR[e]	FNR[f]
Hypo8/31	98.1	97.1	98.6	46.2	1.4
Hypo 9/47	77.8	97.1	97.5	84.6	2.5
Hypo 7/39	84.3	97.1	99.3	23.1	7
Refined Hypo 9/47	97.5	97.1	99.5	18.0	5
Refined Hypo 7/39	94.6	97.2	99.5	15.8	5

[a] ROC: receiver operating characteristic curve.
[b] AUC: area under the curve.
[c] ACC: overall accuracy.
[d] SPC: overall specificity.
[e] TPR: overall true positive rate.
[f] FNR: overall false negative rate.

the hypothesis does not reflect a chance correlation. An additional validation technique based on Fischer's randomization test[30] is found within CATALYST: Cat-Scramble.[22] In this test the biological data and the corresponding structures are scrambled several times and the software is challenged to generate pharmacophoric models from the randomized data. The confidence in the parent hypotheses (i.e., generated from unscrambled data) is lowered proportional to the number of times the software succeeds in generating binding hypotheses from scrambled data of apparently better cost criteria than the parent hypotheses (see Section 4.1.5 Assessment of the Generated Hypotheses in Experimental).[22,25–29]

Eventually, 680 pharmacophore models emerged from 68 automatic HYPOGEN runs, out of which 677 models illustrated Cat. Scramble confidence levels ⩾85%. These successful models were clustered and the best representatives (137 models, Table D under Supplementary data, see Section 4.1.6 Clustering of the Generated

Table 2
Pharmacophoric features and corresponding weights, tolerances and 3D coordinates of Hypo8/31, Hypo9/47 and Hypo7/39

Model	Definitions		Chemical features						
			HBA[e]		HBD[f]		Hbic[g]	Hbic	PosIons[h]
Hypo8/31[a,j]	Weights		2.48		2.48		2.48	2.48	2.48
	Tolerances[d]		1.60	2.20	1.60	2.20	1.60	1.60	1.60
	Coordinates	X	−1.93	−4.11	−3.06	−4.84	−4.61	3.58	2.37
		Y	−0.94	−2.03	0.83	−0.15	5.68	−0.48	3.05
		Z	−3.02	−4.83	−2.13	−4.34	−2.20	−0.38	4.93
Hypo9/47[b]			HBD		Hbic		Hbic	Hbic	RingArom[i]
	Weights		1.86		1.86		1.86	1.86	1.86
	Tolerances		1.60	2.20	1.60	1.60	1.60	1.60	1.60
	Coordinates	X	−0.93	0.72	−2.98	3.80	2.66	−1.34	−3.67
		Y	−2.66	−3.66	−1.38	1.64	2.80	−1.02	−1.14
		Z	−2.04	−4.36	3.40	−2.12	−4.82	1.22	−0.66
Hypo7/39[c]			HBA		Hbic	Hbic	Hbic	Hbic	
	Weights		2.04	2.04	2.04	2.04	2.04	2.04	
	Tolerances		1.60	2.20	1.60	1.60	1.60	1.60	
	Coordinates	X	−5.21	−7.42	5.80	−1.04	4.92	−3.00	
		Y	−4.64	−6.68	4.14	2.14	1.78	−1.30	
		Z	−0.18	−0.18	3.46	−0.28	1.28	−0.64	

[a] Hypo8/31: the 8th pharmacophore hypothesis generated in the 31st HYPOGEN run (Tables C and D under Supplementary data). The model is available as .chm file in the Supplementary data.
[b] Hypo9/47: the 9th pharmacophore hypothesis generated in the 47th HYPOGEN run (Tables C and D under Supplementary data). The model is available as .chm file in the Supplementary data.
[c] Hypo7/39: the 7th pharmacophore hypothesis generated in the 39th HYPOGEN run (Tables C and D under Supplementary data). The model is available as .chm file in the Supplementary data.
[d] Tolerances: refer to the radius of feature spheres.
[e] HBA: hydrogen bond acceptor feature.
[f] HBD: hydrogen bond donor feature.
[g] Hbic: hydrophobic feature.
[h] PosIons: positive ionizable feature.
[i] RingArom: ring aromatic feature.
[j] Hypo8/31 includes 5 exclusion spheres, each of 1.2 Å tolerance, at the following X, Y, Z coordinates: (6.782, −1.976, 4.383), (−0.114, −5.669, −4.343), (−1.033, 5.701, 5.06), (−5.71, 1.332, 6.713), (5.458, 1.028, 3.346).

Pharmacophore Hypotheses) were used in subsequent QSAR modeling. Clearly from Table D under Supplementary data, representative models shared comparable features and acceptable statistical

success criteria. Emergence of several statistically comparable pharmacophore models suggests the ability of CaMKIIδ ligands to assume multiple pharmacophoric binding modes within the
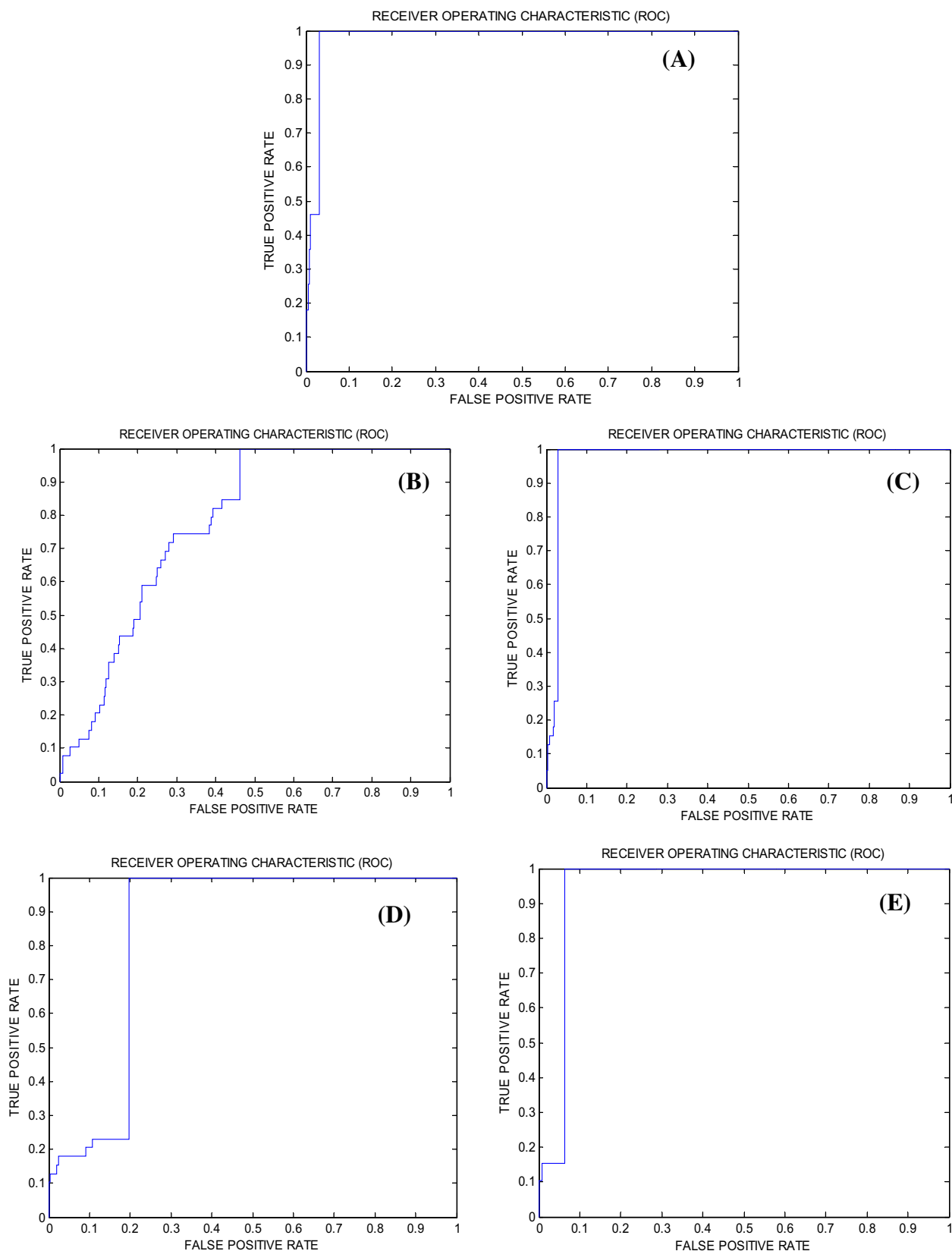

Figure 6. ROC curves of: (A) Hypo8/31, (B) Hypo9/47, (C) sterically-refined Hypo9/47, (D) Hypo7/39, (E) sterically-refined Hypo7/39.

binding pocket. Therefore, it is quite challenging to select any particular pharmacophore hypothesis as a sole representative of the binding process.

2.1.3. QSAR modeling

Despite that pharmacophoric binding hypotheses provide excellent insights into ligand-macromolecule recognition and can be used to mine for new biologically interesting scaffolds, their predictive value as 3D-QSAR models is limited by steric shielding and bioactivity-enhancing or reducing auxiliary groups.[7–19] This point combined with the fact that pharmacophore modeling of CaMKIIδ inhibitors furnished several binding hypotheses of comparable success criteria prompted us to employ classical QSAR analysis to search for the best combination of pharmacophore(s) (i.e., among the best 137 models) and other 2D descriptors capable of explaining bioactivity variation across the whole list of collected inhibitors (**1–88**, Fig. 1 and Table A under Supplementary data). We employed genetic function approximation and multiple linear regression QSAR (GFA-MLR-QSAR) analysis to search for optimal QSAR model (see Section 4.1.7 under Experimental).[7–19,31,32]

The fit values obtained by mapping representative hypotheses (137 models) against collected CaMKIIδ inhibitors were enrolled, together with other physicochemical descriptors (around 250), as independent variables (genes) in GFA-MLR-QSAR analysis. However, since it is essential to access the predictive power of the resulting QSAR models on an external set of inhibitors, we randomly selected 16 molecules (marked with double asterisks in Table A under Supplementary data, see Section 4.1.7 in Experimental) and employed them as external test molecules for validating the QSAR models (r^2_{PRESS}). Moreover, all QSAR models were cross-validated automatically using the leave-one-out cross-validation in CERIUS2.[31,32]

Eq. 1 shows the details of the optimal QSAR model. Figure 2 shows the corresponding scatter plots of experimental versus estimated bioactivities for the training and testing inhibitors.

$$
\begin{aligned}
\mathrm{Log}(1/\mathrm{IC}_{50}) = {} & 3.35 + 17.5 \times 10^{-2}(\mathrm{Hypo8/31}) \\
& + 9.67 \times 10^{-2}(\mathrm{Hypo9/47}) \\
& + 10.8 \times 10^{-2}(\mathrm{Hypo7/39}) \\
& - 9.5 \times 10^{-2}(\mathrm{SdO}) - 3.73(\mathrm{JursFPSA1}) \\
& + 5.41(\mathrm{JursRPSA}) - 0.80(\mathrm{AtypeC28}) \\
& - 8.0 \times 10^{-2}(\mathrm{SaaCH}) \quad r^2_{72} = 0.70, \\
& \text{F-statistic} = 18.19 \quad r^2_{\mathrm{BS}} = 0.59, \\
& r^2_{\mathrm{LOO}} = 0.71, r^2_{\mathrm{PRESS}(16)} = 0.60
\end{aligned}
\tag{1}
$$

where, r^2_{72} is the correlation coefficient against 72 training compounds, r^2_{LOO} is the leave-one-out correlation coefficient, r^2_{BS} is the bootstrapping regression coefficient and r^2_{PRESS} is the predictive r^2 determined for the 16 test compounds.[31,32] Hypo7/39, Hypo8/31 and Hypo9/47 represent the fit values of the training compounds against the 7th, 8th and 9th pharmacophore models generated in the 39th, 31st and 47th automatic HYPOGEN runs shown in Table D under Supplementary data (bolded models in the Table and in figures 3–5). The fit values are calculated via Eq. (D) under Section SM-2 in Supplementary data.

JursFPSA1 is the fractional positively charged partial surface area (calculated by dividing sum of the solvent-accessible surface areas of all positively charged atoms by the total molecular solvent accessible surface area), JursRPSA is the relative polar surface area calculated by dividing total polar surface area by the total molecular solvent-accessible surface area, AtypeC28 is one of the thermodynamic AlogP_atypes family of descriptors and it encodes for the hydrophobic contributions of certain carbon atom types in LogP, SaaCH is an electrotopological state descriptor for aromatic CH
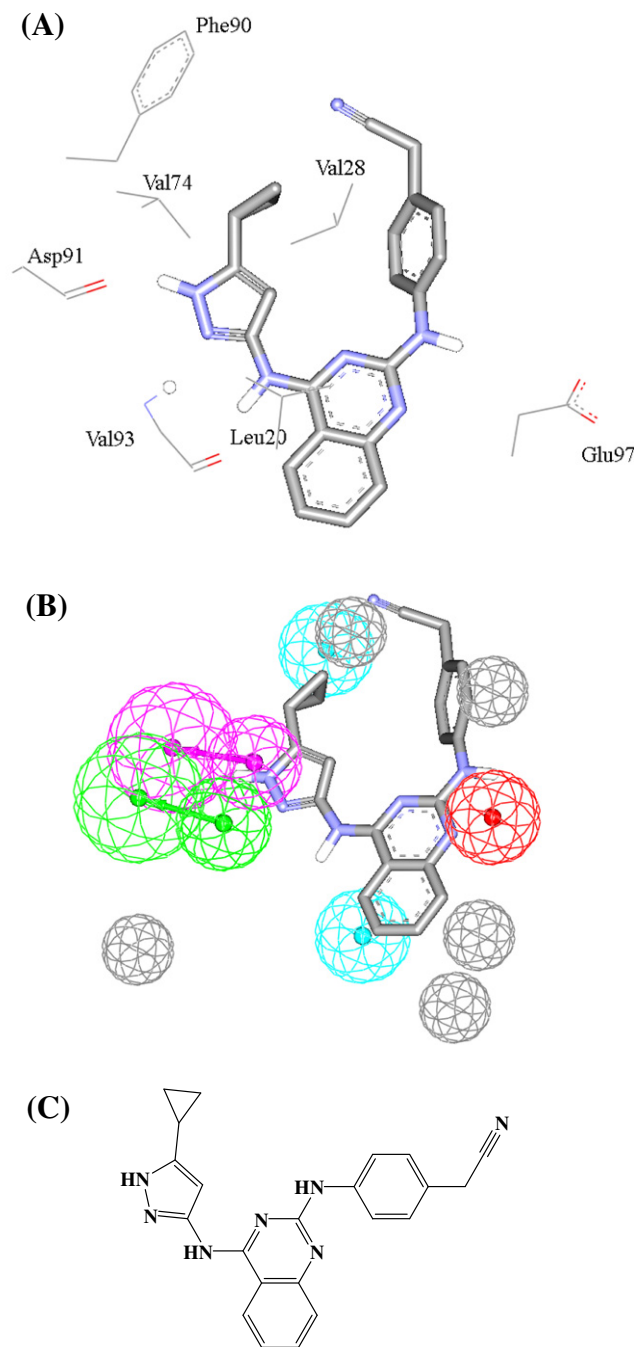

Figure 7. (A) Co-crystallized ligand of CaMKII X-ray structure (PDB code: 2vn9, resolution 2.3 Å). (B) Mapping Hypo8/31 against the co-crystallized ligand of 2vn9 (rigid mapping), (C) the chemical structure of the co-crystallized ligand of 2vn9.

groups, and SdO is the electrotopological state index of carbonyl fragments[31] (see Table E1 in Supplementary data shows the descriptor values for each training and testing compound).

Emergence of three orthogonal pharmacophoric models, that is, Hypo7/39, Hypo8/31 and Hypo9/47, of cross-correlation $r^2 \leqslant 0.21$ (Table 1) in Eq. 1 suggests they represent three complementary binding modes accessible to ligands within the binding pocket of CaMKIIδ, that is, a pharmacophores can optimally explain the bioactivities of some training inhibitors, while the others explain the remaining inhibitors. Similar conclusions were reached about the binding pockets of other targets based on QSAR analysis.[7–19]

Figures 3C and 4C show how Hypo8/31 and Hypo9/47 map **85** (IC₅₀ = 0.009 μM), while Figure 5C shows how Hypo7/39 maps **68**

($IC_{50} = 0.21$ μM). The X, Y, and Z coordinates of the three pharmacophores are shown in Table 2.

Emergence of JursFPSA1 in Eq. 1 in association with significant negative contribution suggests that molecules of diffuse positive charges, that is, over wide surface areas (larger atoms or fragments), disfavor binding to CaMKIIδ compared to molecules of focused positive charges, that is, on smaller-sized fragments, as implied from the emergence of Hypo8/31 (includes a PosIon feature) in Eq. 1. On the other hand, the combined emergence of JursRPSA and SdO, in association with positive and negative regression coefficients, respectively, suggests that compounds of surface-disseminated polarity (of higher JursRPSA values) prefer binding compared to compounds of focused polar areas. For example, carbonyl fragments (e.g., as carboxyl or nitro groups) promote bias towards SdO, and therefore, negatively influences affinity.

The interesting combination of descriptors in Eq. 1 suggests that CaMKIIδ binding pocket is predominantly polar, which explains the superior affinities of ligands having diffuse polarities. This conclusion agrees with negative contributions of the hydrophobic descriptors AtypeC28 and SaaCH in Eq. 1. However, focused polarities (e.g., carbonyl groups) seem to disfavor binding probably due to hydration that competes with binding. On the other hand, the negative effect of diffuse positive charges on affinity suggests that CaMKIIδ binding pocket contains positively-charged residues that repel ligands of diffuse positive charges, while the presence of correctly positioned focused positive groups promote binding through electrostatic attraction with tightly-positioned corresponding negative residue in the binding pocket.

2.2. Receiver operating characteristic (ROC) curve analysis

To further validate the resulting models (both QSAR and pharmacophores), we subjected our QSAR-selected pharmacophores to receiver-operating characteristic (ROC) curve analysis. In ROC analysis, the ability of a particular pharmacophore model to correctly classify a list of compounds as actives or inactives is indicated by the area under the curve (AUC) of the corresponding ROC as well as other parameters, namely, overall accuracy, overall specificity, overall true positive rate and overall false negative rate (see Section 4.1.9 under Experimental for more details).[34–37]

Table 3 and Figure 6 show the ROC results of QSAR-selected pharmacophores. Hypo9/47 and Hypo7/39 illustrated good overall performances with AUC values of 77.8% and 84.3%, respectively. On the other hand, Hypo8/31 exhibited excellent performance with AUC value of 98.1%. This is not unexpected, as presence of positive ionizable, HBD and HBA features in Hypo8/31 should enhance its selectivity compared to Hypo9/47 and Hypo7/39.

The fair overall performances of Hypo9/47 and Hypo7/39 suggest certain degree of promiscuousity.[13] Therefore, we decided to complement the two pharmacophores with exclusion spheres employing HipHop-Refine module of CATALYST.[22] Excluded volumes resemble sterically inaccessible regions within the binding site (see Section 4.1.8 Addition of Exclusion Volumes under Experimental).[33] Accordingly, a structurally diverse training subset was selected for addition of exclusion spheres to Hypo9/47 and Hypo7/39 (see Table F under Supplementary data). The training compounds were selected in such away that the bioactivities of weakly active compounds are explainable by steric clashes within the binding pocket. Figures 4B and 5B show sterically refined versions of Hypo9/47 and Hypo7/39, respectively.

Clearly, the classification performances of sterically-refined versions of Hypo9/47 and Hypo7/39 improved significantly (compared to their unrefined versions) as reflected by their ROC AUC values, which shifted from 77.8% to 97.5% and from 84.3% to 94.6%, respectively, as in Table 3.

2.3. Comparison of Hyp8/31 with the active site of CaMKII

The superiority of Hypo8/31 was further emphasized through its analogy with the binding pocket of CaMKIIδ, i.e., upon analyzing the pharmacophoric features of this model and how it maps a co-crystalized ligand within CaMKIIδ (PDB code: 2vn9, resolution 2.3 Å), as in Figure 7.

Mapping the nitrogens of the aminoquinazoline core of the co-crystallized ligand against PosIon feature in Hypo8/31 (Fig. 7B) corresponds to electrostatic attraction interactions tying the aminoquinazoline with the carboxylic acid of Glu97 (Fig. 7A) in the complex. Similarly, mapping the benzene ring of the ligand's aminoquinazoline core against Hbic feature in Hypo8/31 (Fig. 7B) corresponds to hydrophobic interactions involving this ring with the side chain of Leu20 (Fig. 7A). Moreover, mapping the pyrazole fragment of the co-crystallized ligand against closely positioned HBA and HBD features in Hypo8/31 (Fig. 7B) correlates nicely with hydrogen-bonding interactions connecting the nitrogen atoms of this ring with the peptidic NH and carbonyl groups of Val93 and Asp91 in the co-crystallized complex (Fig. 7A). Finally, fitting the cyclopropyl of the ligand against Hbic feature in Hypo8/31 agrees with positioning this group within a binding pocket composed of the hydrophobic side chains of Phe90, Val74 and Val28, as in Figure 7A.

2.4. In silico screening and subsequent in vitro evaluation

Hypo8/31, sterically-refined Hypo9/47 and Hypo7/39 were employed as 3D search queries against the NCI (238,819 structures)

Table 4
Numbers of selected, filtered, tested, active and inactives hits captured by Hypo8/31 Hypo9/47 and Hypo7/39 from NCI list of compounds[a]

		Number of in silico hits captured by		
		Hypo8/31	Sterically-refined Hypo9/47	Sterically-refined Hypo7/39
Post screening filtering[b]	Before	1823	13165	10697
	After	340	10477	3385
Hits selected based on QSAR predictions		143	683	88
Hits acquired from the NCI[c]		52	57	20
Number of actives[d]		28	26	11
Hits assayed to determine IC_{50}		5	4	1

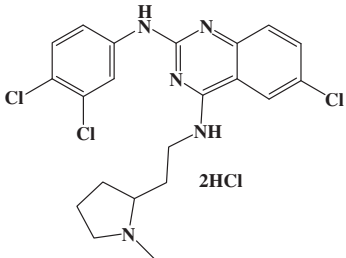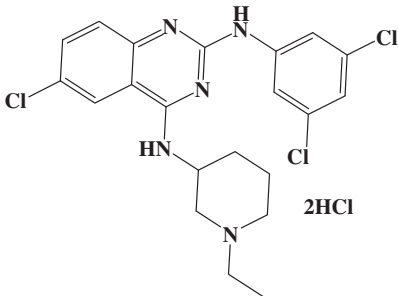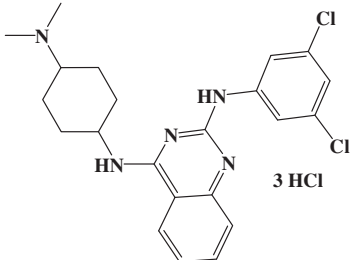[a] NCI: National Cancer Institute list of available compounds (238,819 structures).
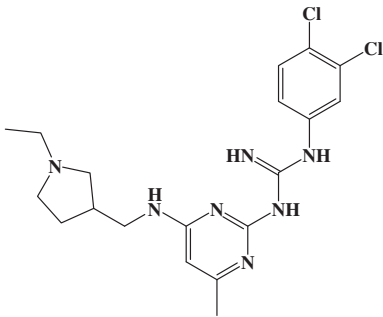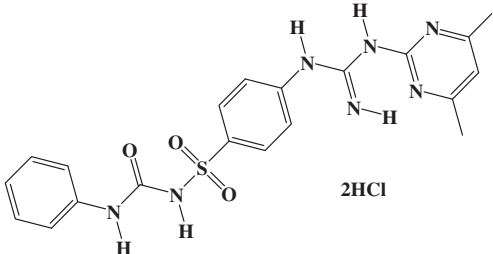
[b] Using Lipinski's and Veber's rules. A maximum of two Lipinski's violations were tolerated.

[c] The total number of acquired hits from the NCI is 68 compounds: 14 were captured by all pharmacophores (Hypo8/31, sterically-refined-Hypo9/47 and sterically-refined-Hypo7/39), 28 were mutually captured by sterically-refined-Hypo9/47 and Hypo8/31, 4 were captured by sterically-refined-Hypo9/47 and sterically-refined-Hypo7/39, and one hit was captured by Hypo 8/31 and sterically-refined-Hypo7/39, the remaining hits were captured by individual pharmacophores.

[d] Compounds illustrating inhibition percentage ≥5% were counted as actives. Total number of active hits is 32 compounds: 11 hits were captured by all three pharmacophores, 11 were captured by both sterically-refined-Hypo9/47 and Hypo8/31. Table H in Supplementary data shows the structures of active hits acquired from NCI, their corresponding QSAR estimates and in vitro anti-CaMKIIδ bioactivities percentages at 10 μM.

Table 5
High-ranking hit molecules with their fit values against Hypo8/31, Hypo9/47, Hypo7/39, their corresponding QSAR estimates from Eq. 1 and their in vitro anti-CaMKIIδ bioactivities

No.	Structure	NCI code	Fit values[a]			QSAR predictions		Experimental	
			Hypo 8/31[b]	Hypo 9/47[c]	Hypo 7/39[d]	log (1/IC$_{50}$)	IC$_{50}$ (µM)	% Inhibition at 10 µM	IC$_{50}$[e] (µM)
89[f,g]		151998	10.7	7.3	0	2.31	0.005	100	0.020
90[f,g]		152189	6.8	6.5	0	1.62	0.024	100	0.082
91[f,g]		143524	6.81	6.26	0	1.22	0.061	86	0.619
92[f,g]		157530	10.0	8.4	5.4	2.92	0.001	77	2.46
93[f,g]		107328	8.8	0	0	−2.47	295	66	1.66

(continued on next page)

Table 5 (*continued*)

No.	Structure	NCI code	Fit values[a]			QSAR predictions		Experimental	
			Hypo 8/31[b]	Hypo 9/47[c]	Hypo 7/39[d]	log (1/IC$_{50}$)	IC$_{50}$ (μM)	% Inhibition at 10 μM	IC$_{50}$[e] (μM)
94[f,g]		142159	6.48	7.57	0	1.06	0.086	83	1.88

[a] Best-fit values calculated by Eq. (D) under Supplementary data.
[b] The maximum fit value in the training set was 11.98 for compound **85** (IC$_{50}$ = 9 nM, the most potent in the collected set).
[c] The maximum fit value in the training set was 9.25 for compounds **51** (IC$_{50}$ = 10 nM, the second most potent among collected compounds) and **52** (IC$_{50}$ = 13 nM, the forth in potency among collected compounds).
[d] The maximum fit value in the training set was 9.96 for **78** (IC$_{50}$ = 42 nM, the 9th in potency rank among collected compounds).
[e] Please refer to figure A under Supplementary data for corresponding dose/response curves and correlation coefficients.
[f] Purity ⩾95% as determined by CHN elemental analysis (see Table G under Supplementary data).
[g] Accurate high resolution mass spectrum corresponds to exact calculated mass (see Table G under Supplementary data).

using the 'Best Flexible Database Search' option implemented within in CATALYST. Compounds that have their chemical groups spatially overlap (map) with corresponding features of the particular pharmacophoric model were captured as hits. Table 4 summarizes the numbers of captured hits by these pharmacophores. Captured hits were filtered based on Lipinski's and Veber's rules.[38,39] Surviving hits were fitted against Hypo8/31, Hypo9/47 and Hypo7/39 (without exclusion volumes) and their fit values, together with other relevant molecular descriptors, were substituted in QSAR Eq. 1 to predict their anti-CaMKIIδ IC$_{50}$ values. The highest-ranking 68 available hits were acquired from the NCI and evaluated in vitro against human recombinant CaMKIIδ assay kit (Cyclex, Japan). Initially, the acquired hits were screened at 10 μM concentrations, subsequently; compounds of anti-CaMKIIδ inhibitory percentages ⩾50% at 10 μM

were further assessed to determine their IC$_{50}$ values. Although 32 hits exhibited measurable anti-CaMKII bioactivities (see Table H under Supplementary data for their structures, QSAR-predictions and experimental bioactivities), only 6 hits exhibited ⩾50% inhibition at 10 μM and were, therefore, evaluated to determine their IC$_{50}$ values (see Figs. C–P under Supplementary data for experimental ^{1}H NMR and mass spectra of acive NCI hits). Figure A under Supplementary data illustrates the dose/response plots of the active hits and standard inhibitor KN-62 under our bioassay conditions.

Table 5 shows the most active hits (**89–94**), their corresponding fit values against Hypo8/31, Hypo9/47, and Hypo7/39, predicted bioactivities based on QSAR Eq. 1, and their in vitro bioactivities. Figures 8 and 9 show hits **89** and **92** and how they map corresponding QSAR-selected pharmacophores. It remains to be
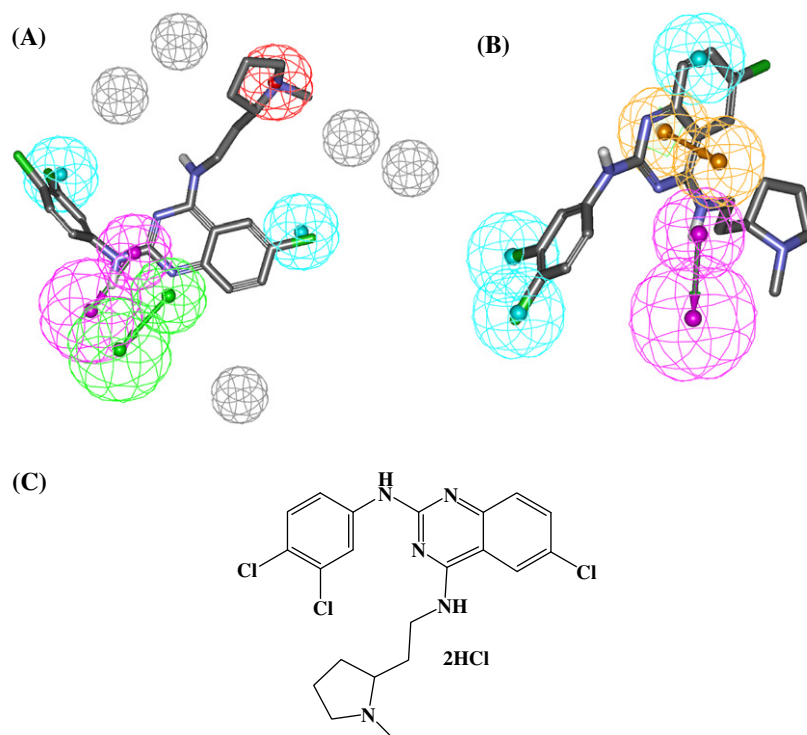

Figure 8. Mapping hit compound **89** (IC$_{50}$ = 20 nM, Table 5) against pharmacophores models (A) Hypo8/31, (B) Hypo9/47, (C) chemical structure of **89** (IC$_{50}$ = 20 nM, Table 5).

mentioned that although the most potent hits, i.e., **89**–**91**, were based on arylaminoquinazoline scaffold (which is not unexpected as it exhibits the HBD/HBA motif that binds the GK+1/GK+3 residues in the hinge of kinases) other less potent hits, e.g., **92** and **93**, exhibit more diverse scaffolds. The diversity of active captured hits is clearly evident in Table H under Supplementary data, which shows the chemical structures, QSAR-predicts and experimental bioactivities of the 32 active hits.

The bioassay procedure was validated by assessing the IC_{50} value of standard inhibitor KN-62[44] via the same assay conditions. It exhibited IC_{50} value of 380 nM, which is rather comparable with the reported literature value (500 nM).[44]

It remains to be mentioned that although QSAR predictions were rather accurate with some hit compounds, i.e., they deviated by a maximum of two logarithmic cycles from experimental bioactivities (e.g., **89**, **90**, and **91**, Table 5), the experimental IC_{50} values of many other hits differed significantly from QSAR predictions. These errors appear to be because of structural differences between training compounds, used in QSAR and pharmacophore modeling, compared to hit molecules. This discrepancy seems to limit the extrapolatory potential of the QSAR equation. On the other hand, success of QSAR equation in predicting the bioactivities of other hits (e.g., **89** and **90**) is probably because they have close chemical similarity to training molecules (e.g., **63**–**88**). Furthermore, the fact that we implemented a different bioassay method from that used for training compounds can also explain part of the predicted-to-experimental differences in hit bioactivities. Additionally, our optimal QSAR model has its own weaknesses; in fact an r^2_{PRESS} of 0.600 suggests certain level of uncertainty in predictions.

2.5. Pharmacophore-guided synthesis of novel CaMKIIδ inhibitors

The fact that pharmacophore Hypo8/31 was significantly superior to Hypo9/47 and Hypo7/39 vis-à-vis their ROC performances and QSAR slopes, prompted us to employ the former model as template for building novel CaMKIIδ inhibitors. Furthermore, the superb potency of NCI hit **89** (IC_{50} = 20 nM, Table 5), which exhibits dual central HBA/HBD, two hydrophobic wings and positive ionizable tail, prompted us to envisage triazine-based analogues as potential CaMKIIδ inhibitors. Triazine rings combine two advantages: (i) facile preparation [46,51–55], and (ii) accessibility to diverse functionalization necessary to satisfy feature-rich nature of Hypo8/31. Moreover, triazine systems can be easily transformed into amino-triazines securing the appropriate juxtapositioned HBA/HBD center required by Hypo8/31. Accordingly, we prepared 12 triazine-based analogues and tested their bioactivities. Table 6 shows the prepared compounds, their predicted and experimental bioactivities.

Syntheses proceeded via sequential nucleophilic aromatic replacements of chloro substituents of cyanuric chloride by anilines and amines, as outlined in Schemes 1–4 [46,51–55]. The first step was performed by nucleophilic aromatic substitution attacks by aniline derivatives, as in Scheme 1. The reaction was performed under −10 °C to 0 °C in acetone to give the mono-amino substituted dichlorotriazine derivatives **95–99** in 44–95% yields. Subsequently, the resulting dichlorotriazine derivatives were treated with alkyl amines, namely, pentyl, isopropyl or ethylamines, in THF under ambient conditions to yield the mono-chlorotriazine derivatives **100–109** in 62–100% yields, as in Scheme 2. Finally,
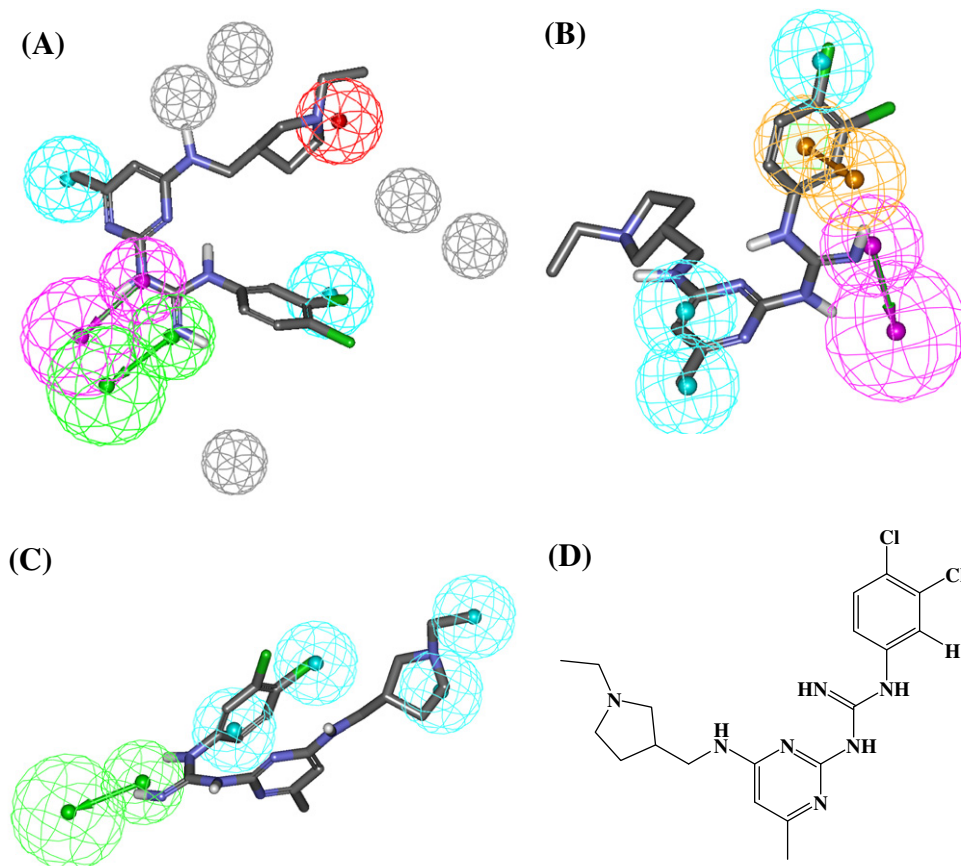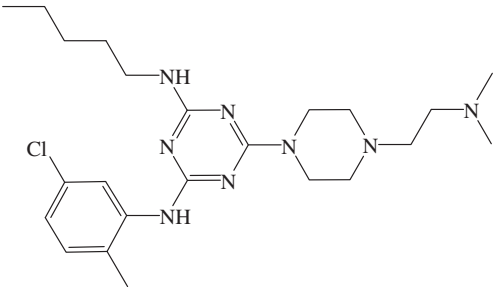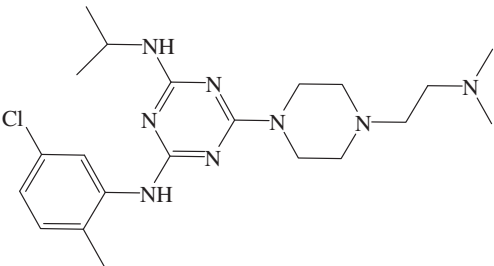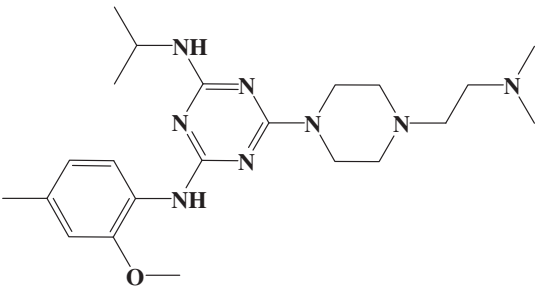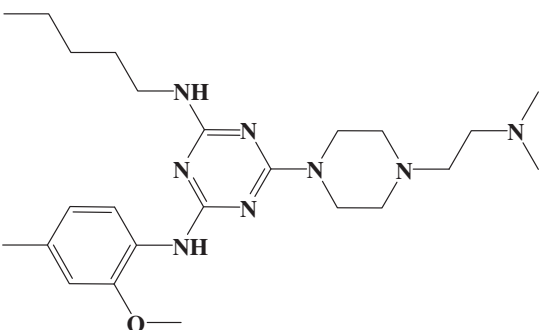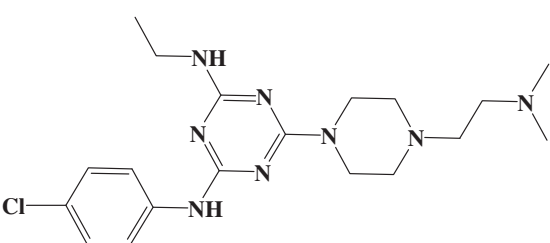
Figure 9. Mapping hit compound **92** (IC_{50} = 2.46 μM, Table 6) against pharmacophores models (A) Hypo8/31; (B) Hypo9/47; (C) Hypo7/39, (D) chemical structure of **92** (IC_{50} = 2.46 μM, Table 5).

Table 6
Synthesized compounds with their fit values against Hypo8/31, Hypo9/47, Hypo7/39, their corresponding QSAR estimates from Eq. 1 and their in vitro anti-CaMKIIδ bioactivities
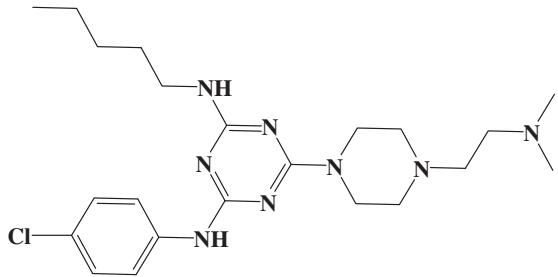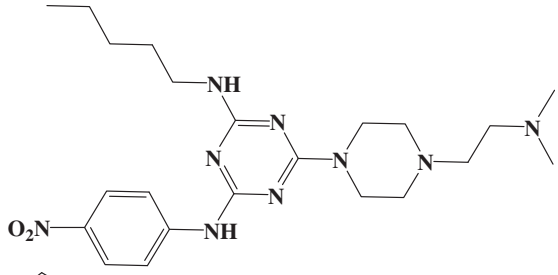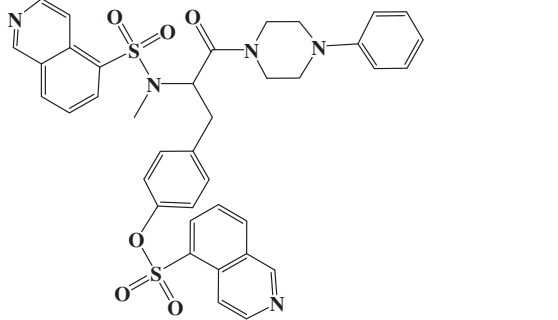
No.[a]	Structure	Fit values[b]			QSAR predictions		Experimental	
		Hypo 8/31	Hypo 9/47	Hypo 7/39	log (1/IC$_{50}$)	IC$_{50}$ (µM)	% Inhibition at 10 µM	IC$_{50}$ (µM)
112		11.64	4.07	0	3.90	0.0001	0	—
113		8.15	5.46	0	3.26	0.0005	0	—
114		8.84	7.07	0	3.17	0.0007	0	—
115		7.44	7.11	0	2.87	0.0014	0	—
116		9.25	5.74	0	2.89	0.0013	0	—

Table 6 (continued)

No.[a]	Structure	Fit values[b]			QSAR predictions		Experimental	
		Hypo 8/31	Hypo 9/47	Hypo 7/39	log (1/IC$_{50}$)	IC$_{50}$ (μM)	% Inhibition at 10 μM	IC$_{50}$ (μM)
117		10.72	7.62	0	3.33	0.0005	40.16	–
118		8.2	5.63	0	2.65	0.0023	1.35	–
119		7.48	6.82	0	2.87	0.0013	0	–
120		10.74	7.82	4.35	3.95	0.0001	0	–
121		7.74	6.40	0	3.16	0.0007	6.88	–

(continued on next page)

Table 6 (continued)

No.[a]	Structure	Fit values[b]			QSAR predictions		Experimental	
		Hypo 8/31	Hypo 9/47	Hypo 7/39	log (1/IC$_{50}$)	IC$_{50}$ (μM)	% Inhibition at 10 μM	IC$_{50}$ (μM)
122		10.18	8.05	0	3.58	0.0003	82	0.401[c]
123		7.04	7.03	0	1.57	0.0271	82	0.154[c]
KN-62		–					85.5	0.380[d]

[a] See Section 4.2 for detailed characterization (NMR, IR, HRMS, Elemental analysis).
[b] Best-fit values calculated by Eq. (D) under Supplementary data.
[c] Please refer to figure B under Supplementary data for corresponding dose/response curves and correlation coefficients.
[d] Please refer to figure A under Supplementary data for corresponding dose/response curves and correlation coefficients.

the resulting mono-chlorotriazines were either refluxed with *t*-Boc-protected piperazine in dioxane to produce **110** and **111** in 70% and 85% yields (Scheme 3), respectively, or were treated with 1-[2-(dimethylamino)ethyl] piperazine in THF at room temperature to produce **114–123** in 9–64% yields, as in Scheme 4. The *t*-Boc-protected piperazine derivatives **110** and **111** were eventually deprotected by methanolic HCl to yield **113** and **113** in 78% and 57% yields, respectively, as shown in Scheme 3. The resulting piperazine-triazine free bases (**114–123**) were dissolved in acetone and eventually precipitated as HCl salts prior to bioassay (see Figs. Q-ZB under Supplementary data for example experimental

^{1}H NMR, ^{13}C NMR and mass spectra of final aminotriazines). This final purification step produced HCl salts at 3 to 5 positions within targeted compounds (**114–123**). These ratios were validated by elemental analyses and in one case, i.e., compound **122**, by argentometric titration of ionic chloride ions (Mohr's method).[56]

The synthesized compounds were bioassayed employing CaM-KII Assay Kit assay (Cyclex, Japan)[40] that was validated by the standard CaMKIIδ inhibitor KN-62.[41]
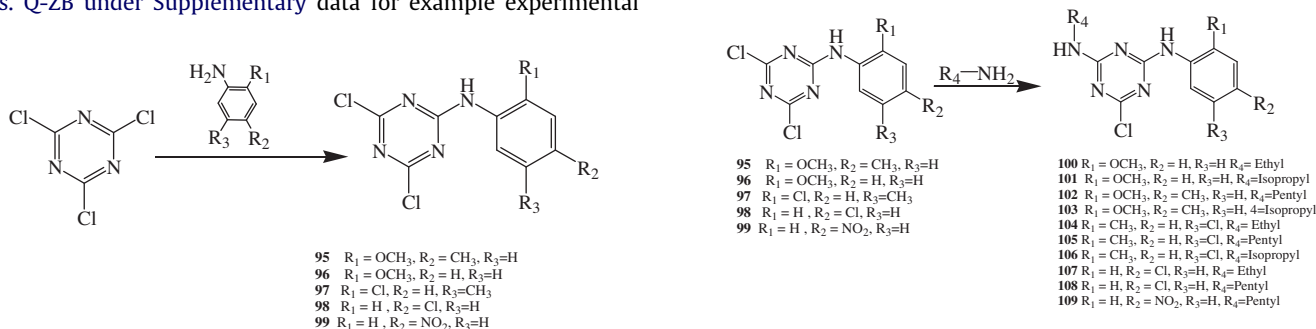
Scheme 1. Synthesis of 4,6-dichloro-1,3,5-triazin-2-ylamino derivatives. The reactions were conducted in acetone at 0 °C.

95 R$_1$ = OCH$_3$, R$_2$ = CH$_3$, R$_3$=H
96 R$_1$ = OCH$_3$, R$_2$ = H, R$_3$=H
97 R$_1$ = Cl, R$_2$ = H, R$_3$=CH$_3$
98 R$_1$ = H , R$_2$ = Cl, R$_3$=H
99 R$_1$ = H , R$_2$ = NO$_2$, R$_3$=H

Scheme 2. Synthesis of 6-chloro-1,3,5-triazin-2,4-diamino derivatives. The reactions were performed I in THF at 0 °C to room temperature using (*i*Pr)$_2$NEt as acid scavenger.

95 R$_1$ = OCH$_3$, R$_2$ = CH$_3$, R$_3$=H
96 R$_1$ = OCH$_3$, R$_2$ = H, R$_3$=H
97 R$_1$ = Cl, R$_2$ = H, R$_3$=CH$_3$
98 R$_1$ = H , R$_2$ = Cl, R$_3$=H
99 R$_1$ = H , R$_2$ = NO$_2$, R$_3$=H

100 R$_1$ = OCH$_3$, R$_2$ = H, R$_3$=H R$_4$= Ethyl
101 R$_1$ = OCH$_3$, R$_2$ = H, R$_3$=H, R$_4$=Isopropyl
102 R$_1$ = OCH$_3$, R$_2$ = CH$_3$, R$_3$=H, R$_4$=Pentyl
103 R$_1$ = OCH$_3$, R$_2$ = CH$_3$, R$_3$=H, 4=Isopropyl
104 R$_1$ = CH$_3$, R$_2$ = H, R$_3$=Cl, R$_4$= Ethyl
105 R$_1$ = CH$_3$, R$_2$ = H, R$_3$=Cl, R$_4$=Pentyl
106 R$_1$ = CH$_3$, R$_2$ = H, R$_3$=Cl, R$_4$=Isopropyl
107 R$_1$ = H, R$_2$ = Cl, R$_3$=H, R$_4$= Ethyl
108 R$_1$ = H, R$_2$ = Cl, R$_3$=H, R$_4$= Pentyl
109 R$_1$ = H, R$_2$ = NO$_2$, R$_3$=H, R$_4$=Pentyl

100 R₁ = OCH₃, R₂ = H, R₃=H R₄= Ethyl
105 R₁ = CH₃, R₂ = H, R₃=Cl, R₄=Pentyl

110 R₁ = OCH₃, R₂ = H, R₃=H R₄= Ethyl
111 R₁ = CH₃, R₂ = H, R₃=Cl, R₄=Pentyl

112 R₁ = OCH₃, R₂ = H, R₃=H R₄= Ethyl
113 R₁ =CH₃ , R₂ = H, R₃=Cl, R₄=Pentyl

Scheme 3. Synthesis of 4-[4-(phenylamino)-6-alkylamino-[1,3,5]triazin-2-yl]-piperazine via 4-[4-(phenylamino)-6-alkylamino-[1,3,5]triazin-2-yl]-piperazine-1-carboxylic acid *tert*-butyl ester. (a) Reflux with piperazine-1-carboxylic acid *tert*-butyl ester in dioxane with (*i*Pr)₂NEt as acid scavenger, (b) methanolic HCl at 0–70 °C.

100 R₁ = OCH₃, R₂ = H, R₃=H R₄= Ethyl
101 R₁ = OCH₃, R₂ = H, R₃=H, R₄=Isopropyl
102 R₁ = OCH₃, R₂ = CH₃, R₃=H, R₄=Pentyl
103 R₁ = OCH₃, R₂ = CH₃, R₃=H, 4=Isopropyl
104 R₁ = CH₃, R₂ = H, R₃=Cl, R₄= Ethyl
105 R₁ = CH₃, R₂ = H, R₃=Cl, R₄=Pentyl
106 R₁ = CH₃, R₂ = H, R₃=Cl, R₄=Isopropyl
107 R₁ = H, R₂ = Cl, R₃=H, R₄= Ethyl
108 R₁ = H, R₂ = Cl, R₃=H, R₄= Pentyl
109 R₁ = H, R₂ = NO₂, R₃=H, R₄=Pentyl

114 R₁ = OCH₃, R₂ = H, R₃=H R₄= Ethyl
115 R₁ = OCH₃, R₂ = H, R₃=H, R₄=Isopropyl
116 R₁ = CH₃, R₂ = H, R₃=Cl, R₄= Ethyl
117 R₁ = CH₃, R₂ = H, R₃=Cl, R₄=Pentyl
118 R₁ = CH₃, R₂ = H, R₃=Cl, R₄=Isopropyl
119 R₁ = OCH₃, R₂ = CH₃, R₃=H, R₄=Isopropyl
120 R₁ = OCH₃, R₂ = CH₃, R₃=H, R₄=Pentyl
121 R₁ = H, R₂ = Cl, R₃=H, R₄= Ethyl
122 R₁ = H, R₂ = Cl, R₃=H, R₄=Pentyl
123 R₁ = H, R₂ = NO₂, R₃=H, R₄=Pentyl

Scheme 4. Synthesis of 6-[4-(2-dimethylamino-ethyl)-piperazin-1-yl]-*N*-(3-phenyl)-*N*′-alkyl-[1,3,5]triazine-2,4-diamine derivatives. (a) 1-[2-(Dimethylamino) ethyl] piperazine in THF at 25 °C using triethylamine as acid scavenger.

Table 6 shows the prepared compounds and their corresponding predicted and experimental bioactivities. Clearly from the table, all prepared final products (**114–123**) successfully mapped Hypo8/31 and were predicted by QSAR Eq. 1 to have potent anti-CaMKII bioactivities. However, only 2 illustrated significant experimental potencies (**122** and **123**, Table 6) ranging from submicromolar to nanomolar IC₅₀ values against CaMKII.

Clearly from Table 6, the experimental bioactivities of prepared compounds differ significantly from their QSAR-based predictions. Nevertheless, we believe it is possible to explain these deviations through the following points: (i) The poor activities of ethyl and isopropyl substituted triazines (e.g., **114**, **115**, **116**, **119**, and **121**) compared to pentyl-substituted analogues (**117**, **122**, and **123**) seem to be because the later can optimally fit Hypo8/31 in at least two distinct poses compared to a single optimal pose for ethyl and isopropyl substituted analogues. Freedom in mapping Hypo8/31 in different poses suggests lesser entropic cost upon binding for the pentyl analogues explaining their higher affinities. Figure 0A–F illustrate this point. (ii) The inactivities of *o*-anisidine-based triazines (i.e., **112**, **114**, **115**, **119** and **120**) can be attributed to the formation of intermolecularly hydrogen-bonded 5-membered rings involving the *o*-anisidine OMe and amino-triazine NH. This deprives the NH from its hydrogen-bond donor character leading to the apparent loss of activity of these analogues. Figure 10G, H, and I illustrate this point in the case **121**. (iii) The inferior anti-CaMKII bioactivities of unsubstituted piperzine analogues (i.e., **112** and **113**) compared to those dimethyl aminoethyl-substituted piperazine analogues (i.e., **122** and **123**) can be explained based on the

less-than-optimal mapping of the PosIon feature of the unsubstituted piperazine analogues compared to their *N*-dimethyl aminoethyl-piperazine counterparts. Figure 11 clearly explains this point.

3. Conclusions

CaMKIIδ inhibitors are currently considered as potential treatments for cardiovascular disease. The pharmacophoric space of CaMKIIδ inhibitors was explored via nine diverse sets of inhibitors and using CATALYST-HYPOGEN to identify high quality binding model(s). Subsequently, genetic algorithm and multiple linear regression analysis were employed to access optimal QSAR model capable of explaining anti-CaMKIIδ bioactivity variation across 88 collected CaMKIIδ inhibitors. Three orthogonal pharmacophoric models emerged in the QSAR equation suggesting the existence of at least three distinct binding modes accessible to ligands within CaMKIIδ binding pocket. The QSAR equation and the associated pharmacophoric models were experimentally validated by the identification of several CaMKIIδ inhibitors retrieved via in silico screening. The QSAR equation and the associated pharmacophoric models were used to guide synthetic exploration of a triazine based new series of CaMKIIδ inhibitors that resulted in several novel nanomolar CaMKIIδ inhibitors.

4. Experimental

4.1. Molecular modeling

4.1.1. Software and hardware

The following software packages were utilized in the present research.

- CATALYST (Version 4.11), Accelrys Inc. (www.accelrys.com), USA.
- CERIUS2 (Version 4.10), Accelrys Inc. (www.accelrys.com), USA.
- CS ChemDraw Ultra 6.0, Cambridge Soft Corp. (http://www.cambridgesoft.Com), USA.
- Discovery Studio 2.5, Accelrys Inc. (www.accelrys.com), USA.

Pharmacophore and QSAR modeling studies were performed using CATALYST (HYPOGEN module) and CERIUS2 software suites from Accelrys Inc. (San Diego, California, www.accelrys.com) installed on a Silicon Graphics Octane2 desktop workstation equipped with a dual 600 MHz MIPS R14000 processor (1.0 GB RAM) running the Irix 6.5 operating system. Structure drawing was performed employing ChemDraw Ultra 6.0 which was installed on a Pentium 4 PC.

4.1.2. Data set

The structures of 88 CaMKIIδ inhibitors (**1–88**, Fig. 1 and Table A under Supplementary data) were collected from recently published
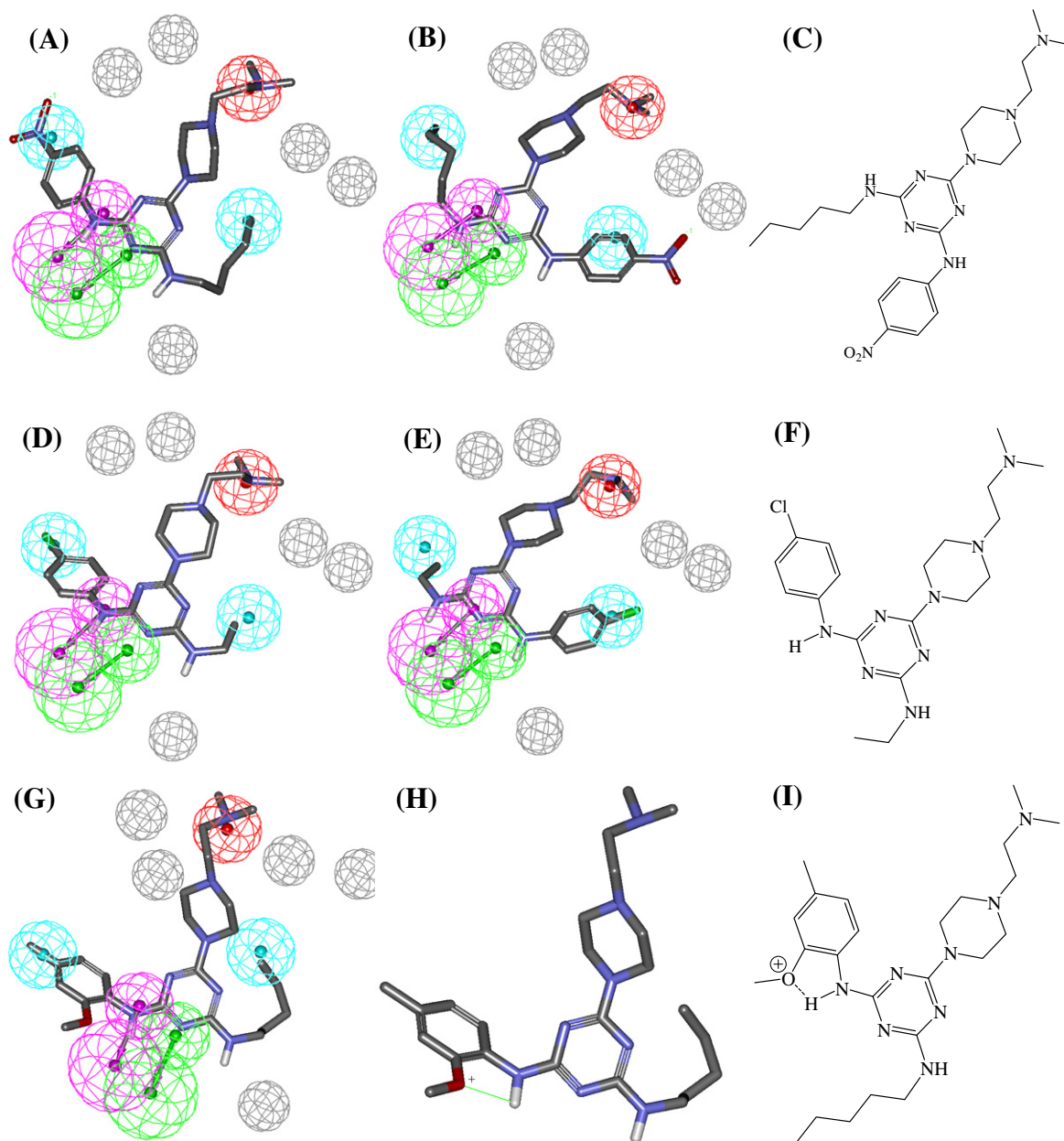
Figure 10. (A) and (B) two optimal alternative mappings of Hypo8/31 against synthesized compound **123** (IC$_{50}$ = 0.154 μM), (C) chemical structure of **123**. (D) and (E) similar, but suboptimal (the ethyl is not mapped in **E**), mappings of Hypo8/31 against synthesized compound **121** (inhibition at 10 μM = 6.8%), (F) chemical structure of **121**. (G) Proposed mapping of **120** ((inhibition at 10 μM = 0%) against Hypo8/31, (H) intermolecular hydrogenbonding involving the *o*-methoxy O and amino-triazine NH in **120** which seems to deprive the amino-triazine NH from fitting the HBD feature in Hypo8/31, (I) chemical structure of **120**.

literature.[5,6,20,21] Although the in vitro bioactivities of the collected inhibitors were gathered from four separate articles they were determined employing the same bioassay methodologies. The bioactivities were expressed as the concentrations of the test compounds that inhibited the activity of CaMKIIδ by 50% (IC$_{50}$, μM). The logarithm of measured IC$_{50}$ (μM) values were used in the three-dimensional quantitative structure activity analysis (3D-QSAR), thus correlating the data linear to the free energy change.

In cases where IC$_{50}$ is expressed as being higher than 20 μM (e.g., compounds **4**, **8**, **14**, **29**, **79** and **80**, see Table A under Supplementary data) it was assumed it equals 210 μM. This assumption is necessary to allow 3.5 log cycles separation between the most potent training compound (i.e., **85**) and the least active training compounds (i.e., **4**, **8**, **14**, **29**, **79** and **80**). This is necessary for pharmacophore modeling in CATALYST. Moreover, this assumption is

necessary to allow statistical correlation and QSAR analysis since regression requires exact values. The logarithmic transformation of IC$_{50}$ values should minimize any potential errors resulting from this assumption.

The two-dimensional (2D) chemical structures of the inhibitors were sketched using ChemDraw Ultra and saved in MDL-molfile format. Subsequently, they were imported into CATALYST, converted into corresponding standard 3D structures and energy minimized to the closest local minimum using the molecular mechanics CHARMm force field implemented in CATALYST. The resulting 3D structures were utilized as starting conformers for CATALYST conformational analysis.

4.1.3. Conformational analysis

The molecular flexibilities of the collected compounds were taken into account by considering each compound as a collection
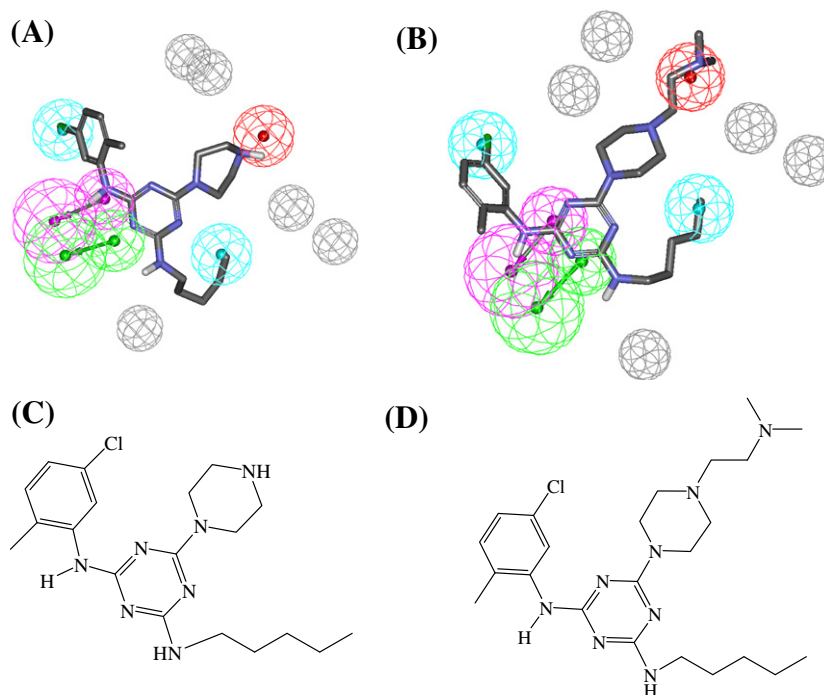
Figure 11. (A) and (B) show Hypo8/31 fitted against synthesized compounds **113** (inhibition at 10 μM = 0%) and **117** (inhibition at 10 μM = 40.16%), respectively, (C) and (D) show the chemical strcutres of **113** and **117**, respectively.

of conformers representing different areas of the conformational space accessible to the molecule within a given energy range. Accordingly, the conformational space of each inhibitor (**1–88**, Fig. 1 and Table A under Supplementary data) was explored adopting the 'best conformer generation' option within CATALYST[22] based on the generalized CHARMm force field implemented in the program. Default parameters were employed in the conformation generation procedure of training compounds, i.e., a conformational ensemble was generated with an energy threshold of 20 kcal/mol from the local minimized structure at which has the lowest energy level and a maximum limit of 250 conformers per molecule.[22]

4.1.4. Pharmacophoric hypotheses generation

All 88 molecules with their associated conformational models were regrouped into a spreadsheet. The biological data of the inhibitors were reported with an 'Uncertainty' value of 3, which means that the actual bioactivity of a particular inhibitor is assumed to be situated somewhere in an interval ranging from one-third to three-times the reported bioactivity value of that inhibitor.[26,28] Subsequently, nine structurally diverse training subsets were carefully selected from the collection for pharmacophore modeling (sets **I**, **II**, **III**, **IV**, **V**, **VI**, **VII**, **VIII** and **IX** in Table B under Supplementary data). Typically, CATALYST requires informative training sets that include at least 16 compounds of evenly spread bioactivities over at least three and a half logarithmic cycles. Lesser training lists could lead to chance correlation and thus faulty models.

The selected training sets were utilized to conduct 68 modeling runs to explore the pharmacophoric space of CaMKIIδ inhibitors (Table C under Supplementary data). The exploration process included altering interfeature spacing parameter (100 and 300 picometers) and the maximum number of allowed features in the resulting pharmacophore hypotheses, i.e., they were allowed to vary from 4 to 5 for first and second runs and from 5 to 5 for third and fourth runs of each training set, as shown in Table C under Supplementary data. Moreover, the interfeature distances were allowed

to vary from 100 to 300 picometers (Table C under Supplementary data). Exploration trials yielded 680 models. Pharmacophore modeling employing CATALYST proceeds through three successive phases: the constructive phase, subtractive phase and optimization phase (see CATALYST Modeling Algorithm in Section SM-1 under Supplementary data).[22,25–29]

4.1.5. Assessment of the generated hypotheses

When generating hypotheses, CATALYST attempts to minimize a cost function consisting of three terms: Weight cost, Error cost and Configuration cost (see Section SM-2 under Supplementary data).

An additional approach to assess the quality of CATALYST-HYPOGEN pharmacophores is to cross-validate them using the Cat-Scramble program implemented in CATALYST. This validation procedure is based on Fisher's randomization test.[30] In this validation test; we selected a 95% confidence level, which instruct CATALYST to generate 19 random spreadsheets by the Cat-Scramble command. Subsequently, CATALYST-HYPOGEN is challenged to use these random spreadsheets to generate hypotheses using exactly the same features and parameters used in generating the initial unscrambled hypotheses. Success in generating pharmacophores of comparable cost criteria to those produced by the original unscrambled data reduces the confidence in the training compounds and the unscrambled original pharmacophore models.[22,30,43] Based on Fisher randomization criteria; 677 pharmacophores exceeded the 85% significance threshold for subsequent processing (clustering and QSAR analyses).

4.1.6. Clustering of the generated pharmacophore hypotheses

The successful models (677) were clustered into 134 groups (one representative per five closely related models) utilizing the hierarchical average linkage method available in CATALYST. Subsequently, the highest-ranking representatives, as judged based on their significance r^2-values, were selected to represent their corresponding clusters in subsequent QSAR modeling. Table D under Supplementary data shows information about representative

pharmacophores including their pharmacophoric features, success criteria and differences from corresponding null hypotheses. The table also shows the corresponding Cat. Scramble confidence levels for each representative pharmacophore.

4.1.7. QSAR modeling

A subset of 72 compounds from the total list of inhibitors (**1–88**, Fig. 1 and Table A under Supplementary data) was utilized as a training set for QSAR modeling; the remaining 16 molecules (ca. 20% of the dataset) were employed as an external test subset for validating the QSAR models. The test molecules were selected as follows: the 88 inhibitors were ranked according to their IC_{50} values, and then every fifth compound was selected for the test set starting from the high-potency end. This selection considers the fact that the test molecules must represent a range of biological activities similar to that of the training set. The selected test inhibitors are marked with double asterisks in Table A under Supplementary data.

The logarithm of measured $1/IC_{50}$ (μM) values was used in QSAR, thus correlating the data linear to the free energy change. The chemical structures of the inhibitors were imported into CERIUS2 as standard 3D single conformer representations in SD format. Subsequently, different descriptor groups were calculated for each compound employing the C2.DESCRIPTOR module of CERIUS2. The calculated descriptors included various simple and valence connectivity indices, electro-topological state indices and other molecular descriptors (e.g., logarithm of partition coefficient, polarizability, dipole moment, molecular volume, molecular weight, molecular surface area, etc.).[31] The training compounds were fitted (using the best-fit option in CATALYST)[22] against the representative pharmacophores (134 models, Table D under Supplementary data), and their fit values were added as additional descriptors. The fit value for any compound is obtained automatically via Eq. D in Section SM-1 under Supplementary data. [22]

Genetic function approximation (GFA) was employed to search for the best possible QSAR regression equation capable of correlating the variations in biological activities of the training compounds with variations in the generated descriptors, i.e., multiple linear regression modeling (MLR). GFA techniques rely on the evolutionary operations of 'crossover and mutation' to select optimal combinations of descriptors (i.e., chromosomes) capable of explaining bioactivity variation among training compounds from a large pool of possible descriptor combinations, i.e., chromosomes population. However, to avoid overwhelming GFA-MLR with large number of poor descriptor populations, we removed lowest-variance descriptors (20%) prior to QSAR analysis.

Each chromosome is associated with a fitness value that reflects how good it is compared to other solutions. The fitness function employed herein is based on Friedman's 'lack-of-fit' (LOF).[31]

Our preliminary diagnostic trials suggested the following optimal GFA parameters: explore linear, quadratic and spline equations at mating and mutation probabilities of 50%; population size = 500; number of genetic iterations = 30,000 and lack-of-fit (LOF) smoothness parameter = 1.0. However, to determine the optimal number of explanatory terms (QSAR descriptors), it was decided to scan and evaluate all possible QSAR models resulting from 5 to 25 explanatory terms.

All QSAR models were validated employing leave one-out cross-validation (r_{LOO}^2), bootstrapping (r_{BS}^2) and predictive r^2 (r_{PRESS}^2) calculated from the test subsets. The predictive r_{PRESS}^2 is defined as in Eq. 2:

$$r_{PRESS}^2 = SD - PRESS/SD \qquad (2)$$

where SD is the sum of the squared deviations between the biological activities of the test set and the mean activity of the training set molecules, PRESS is the squared deviations between predicted and actual activity values for every molecule in the test set.

4.1.8. Addition of exclusion volumes

To account for the steric constrains of the binding pocket we decided to decorate Hypo9/47 and Hypo7/39 with exclusion volumes employing HipHop-Refine module of CATALYST. HipHop-Refine uses inactive training compounds to construct excluded volumes that resemble the steric constrains of the binding pocket. It identifies spaces occupied by the conformations of inactive compounds and free from active ones. These regions are then filled with excluded volumes.[9–11,15,22]

A subset of 23 compounds (Table F under Supplementary data) was used for constructing appropriate exclusion regions around Hypo9/47 and Hypo7/39.

In HipHop-Refine the user defines how many molecules must map completely or partially the particular hypothesis via the Principal and Maximum Omitted Features (MaxOmitFeat) parameters. Active compounds are normally assigned MaxOmitFeat parameter of zero and principal value of 2 to instruct the software to consider all their chemical moieties in pharmacophore modeling and to fit them against all the pharmacophoric features of a particular hypothesis. On the other hand, inactive compounds are allowed to miss one (or two) features by assigning them a MaxOmitFeat of 1 (or 2) and principal value of zero.

We decided to consider 20 μM as an appropriate activity/inactivity threshold. Accordingly, inhibitors of IC_{50} values $\leqslant 20\,\mu$M were regarded as 'actives' and were assigned principal and MaxOmitFeat values of 2 and 0, respectively, On the other hand, inhibitors of IC_{50} >20 μM were considered inactive and were assigned principal values of zero.[22]

On the other hand, inhibitors of IC_{50} values ranging from 0.080 to 20 μM were considered as intermediates and were assigned Principal values of 1 and MaxOmitFeat parameter of 1 (rarely 0 or 2). While inhibitors of IC_{50} values >20 μM were regarded as inactives and were assigned a Principal value of 0. However, each inactive compound was carefully evaluated to assess whether its low potency is attributable to missing one or more pharmacophoric features, i.e., compared to active compounds, or related to possible steric clashes within the binding pocket, or due to both factors. Therefore, inactive compounds suspected of missing one or more pharmacophoric features were assigned MaxOmitFeat values of 1 or 2, respectively. Spaces occupied by conformers and/or mappings of this group of compounds and free from conformers and/or mappings of active compounds are filled with excluded volumes. However, compounds that seem to be inactive mainly due to steric clashes within the binding pocket were assigned MaxOmitFeat value of zero. This value instructs HipHop-Refine to force inactive compound(s) to map all the pharmacophoric features of the binding model, and therefore permits the software to identify spaces occupied by excess structural fragments/features of such inactive compounds and fill them with excluded volumes.[9] HipHop-Refine was configured to allow a maximum of 100 exclusion spheres to be added to Hypo9/47 and Hypo7/39. Table F, under Supplementary data, shows the training compounds employed in this step and their corresponding principal and MaxOmitFeat parameters.

4.1.9. Receiver operating characteristic (ROC) curve analysis

Selected pharmacophore models (i.e., Hypo8/31, Hypo7/39 and Hypo 9/47) were validated by assessing their abilities to selectively capture diverse CaMKII active compounds from a large testing list of actives and decoys.

The testing list was prepared as described by Verdonk and co-workers.[34] Briefly, decoy compounds were selected based on three basic one-dimensional (1D) properties that allow the

assessment of distance (D) between two molecules (e.g., i and j): (1) the number of hydrogen-bond donors (NumHBD); (2) number of hydrogen-bond acceptors (NumHBA) and (3) count of nonpolar atoms (NP, defined as the summation of Cl, F, Br, I, S and C atoms in a particular molecule). For each active compound in the test set, the distance to the nearest other active compound is assessed by their Euclidean Distance (Eq. 3):

$$D(i,j) = \sqrt{(NumHBD_i - NumHBD_j)^2 + (NumHBA_i - NumHBA_j)^2 + (NP_i - NP_j)^2}$$
(3)

The minimum distances are then averaged over all active compounds (Dmin). Subsequently, for each active compound in the test set, around 30 decoys were randomly chosen from the ZINC database.[36] The decoys were selected in such a way that they did not exceed Dmin distance from their corresponding active compound.

To diversify active members in the list, we excluded any active compound having zero distance $(D(i,j))$ from other active compound(s) in the test set. Active testing compounds were defined as those possessing CaMKII affinities ranging from 0.009 to 15.02 μM. The test set included 39 active compounds and 1307 ZINC decoys.

The test set (1346 compounds) was screened by each particular pharmacophore employing the 'Best flexible search' option implemented in CATALYST, while the conformational spaces of the compounds were generated employing the 'Fast conformation generation option' implemented in CATALYST. Compounds missing one or more features were discarded from the hit list. In silico hits were scored employing their fit values as calculated by Eq. D in Supplementary data.

The ROC curve analysis describes the sensitivity (Se or true positive rate, Eq. 4) for any possible change in the number of selected compounds (n) as a function of (1-Sp, or false positive rate). Sp is defined as specificity or true negative rate (Eq. 5). [47,49]

$$Se = \frac{\text{Number of Selected Actives}}{\text{Total Number of Actives}} = \frac{TP}{TP + FN}$$
(4)

$$Sp = \frac{\text{Number of Discarded Inactives}}{\text{Total Number of Inactives}} = \frac{TN}{TN + FP}$$
(5)

where, TP is the number of active compounds captured by the virtual screening method (true positives), FN is the number of active compounds discarded by the virtual screening method, TN is the number of discarded decoys (presumably inactives), while FP is the number of captured decoys (presumably inactive).[47,49]

If all molecules scored by a virtual screening (VS) protocol with sufficient discriminatory power are ranked according to their score (i.e., fit values), starting with the best-scored molecule and ending with the molecule that got the lowest score, most of the actives will have a higher score than the decoys. Since some of the actives will be scored lower than decoys, an overlap between the distribution of active molecules and decoys will occur, which will lead to the prediction of false positives and false negatives.[47,49] The selection of one score value as a threshold strongly influences the ratio of actives to decoys and therefore the validation of a VS method. The ROC curve method avoids the selection of a threshold by considering all Se and Sp pairs for each score threshold.[47,49] A ROC curve is plotted by setting the score of the active molecule as the first threshold. Afterwards, the number of decoys within this cutoff is counted and the corresponding Se and Sp pair is calculated. This calculation is repeated for the active molecule with the second highest score and so forth, until the scores of all actives are considered as selection thresholds.

The success of a particular virtual screening workflow can be judged from the following criteria (shown in Table 3):

(1) Area under the ROC curve (AUC).[47,49,56]

Overall accuracy (ACC), which describes the percentage of correctly classified molecules by the screening protocol (Eq. 6).[47,49,57]

$$ACC = \frac{TP + TN}{N} = \frac{A}{N} \cdot Se + \left(1 - \frac{A}{N}\right) \cdot Sp$$
(6)

where, N is the total number of compounds in the testing database, A is the number of true actives in the testing database.

(3) Overall specificity (SPC): describes the percentage of discarded inactives by the particular virtual screening workflow.[47,49,57]

(4) Overall true positive rate (TPR or overall sensitivity): describes the fraction percentage of captured actives from the total number of actives.[47,49,57]

(5) Overall false negative rate (FNR or overall percentage of discarded actives): describes the fraction percentage of active compounds discarded by the virtual screening method.[47,49,57]

4.1.10. In silico screening for new CaMKIIδ inhibitors

Hypo8/31 and the sterically refined versions of Hypo9/47 and Hypo7/39 were employed as 3D search queries to screen the NCI 3D flexible structural database. The screening was done employing the 'Best Flexible Database Search' option implemented within CATALYST. NCI hits were filtered according to Lipinski's[38] and Veber's[39] rules, as in Table 4. Remaining hits were fitted against the three pharmacophores using the 'best fit' option within CATALYST. The fit values together with the relevant molecular descriptors of each hit were substituted in the optimal QSAR Eq. 1. The highest ranking molecules based on QSAR predictions were acquired and tested in vitro. Table 5 shows active hits and their QSAR-predictions and experimental bioactivities.

4.2. Synthesis of triazine analogues

4.2.1. General synthetic procedures

Melting points were measured using Gallenkampf melting point apparatus and are uncorrected. ^{1}H NMR and ^{13}C NMR spectrums were collected on a Bruker NMR400 spectrometer. High resolution mass spectrometry was performed using LC Mass Bruker Apex-IV mass spectrometer utilizing an electrospray interface. Infrared spectra were recorded using Shimadzu IR Affinity-1 spectrophotometer. The samples were analyzed as KBr pellets. Analytical thin layer chromatography (TLC) was carried out using pre-coated aluminum plates and visualized by UV light (at 254 and/or 360 nm). Elemental analysis was performed using EuroVector elemental analyzer. Chemicals and solvents were used without further purification.

4.2.2. Preparation of 4,6-dichloro-1,3,5-triazin-2-ylamino derivatives (95–99, Scheme 1)

To a magnetically-stirred, ice-bathed, solution of substituted aniline (1 equiv) in acetone (20 mL) at 0 °C was added cyanuric chloride (1 equiv), and the resulting mixture was stirred at 0 °C for 2 h and then at room temperature for an additional 2 h. Subsequently, crushed ice (10 mL) was added to the reaction, and the mixture was allowed to warm up to room temperature over 1 h. The solid was collected by vacuum filtration and was washed with water three times (3–10 mL).[45]

4.2.2.1. (4,6-Dichloro-[1,3,5]triazin-2-yl)-(2-methoxy-4-methyl-phenyl)-amine (95).

Prepared from commercially available 4-methyl o-anisidine (3.321 g, 27 mmol) and cyanuric chloride (5 g, 27 mmol) to yield **95** as cream colored powder (3.4 g, 44%). Mp: 176 °C from acetone, v_{max} (KBr disc) 3381, 1724, 1620,

1579 cm^{-1}; ^{1}H NMR (400 MHz, DMSO-d_6, rotameric[45]): δ 2.24 (s, 3H, CH$_3$), 3.73 (s, 3H, OCH$_3$), 6.98 (m, 1H), 7.07 (m, 1H), 7.14 (s, 1H), and 10.46 (s, 1H, NH) ppm; ^{13}C NMR (100 MHz, DMSO-d_6): δ 22.70 (CH$_3$), 58.42 (OCH$_3$), 114.88 (CH), 126.77 (C), 129.84 (CH), 131.07 (CH), 131.91 (C), 154.09 (C), 167.59 (C), 171.50 and 172.24 (C, rotamer splitting) ppm. HRMS-ESI m/z [M+H]$^+$ calcd for C$_{11}$H$_{11}$Cl$_2$N$_4$O: 285.03044, found: 285.03040. Anal. Calcd for C$_{11}$H$_{10}$Cl$_2$N$_4$O: C, 46.34; H, 3.54; N, 19.65. Found: C, 46.39; H, 3.37; N, 19.29.

4.2.2.2. (4,6-Dichloro-[1,3,5]triazin-2-yl)-(2-methoxy-phenyl)-amine (96).
Prepared from commercially available *o*-anisidine (0.74 g, 5.4 mmol) and cyanuric chloride (1 g, 5.4 mmol) to yield **96** as cream colored powder (0.75 g, 51%). Mp: 171 °C from acetone (lit. mp: 175 °C from CCl$_4$);[50] v_{max} (KBr disc) 3393, 1608, 1570 cm^{-1}, ^{1}H NMR (400 MHz, DMSO-d_6): δ 3.78 (s, 3H, OCH$_3$), 6.96 (m, 1H), 7.12 (m, 1H), 7.26 (m, 1H), 7.39 (m, 1H), and 10.48 (s, 1H, NH) ppm; ^{13}C NMR (100 MHz, DMSO-d_6, rotameric[45]): δ 58.37 (OCH$_3$), 114.88 (CH), 122.97 (CH), 126.95 (C), 129.35 (CH), 130.75 (CH), 156 (C), 167.49 (C), 171.54 and 172.25 (C, rotamer splitting) ppm. HRMS-ESI m/z [M+H]$^+$ calcd for C$_{10}$H$_9$Cl$_2$N$_4$O: 271.01479, found: 271.01470. Anal. Calcd for C$_{10}$H$_8$Cl$_2$N$_4$O: C, 44.30; H, 2.97; N, 20.67. Found: C, 42.81; H, 3.07; N, 19.57.

4.2.2.3. (5-Chloro-2-methyl-phenyl)-(4,6-dichloro-[1,3,5]triazin-2-yl)-amine (97).
Prepared from commercially available 5-chloro-2-methyl-aniline (0.78 g, 5.4 mmol) and cyanuric chloride (1.0 g, 5.4 mmol) to yield **97** as rose colored powder (1.16 g, 74%). Mp: 192.5 °C from acetone (lit. mp: 192–193)[51]; v_{max} (KBr disc) 3225, 1608, 1587 cm^{-1}, ^{1}H NMR (400 MHz, DMSO-d_6): δ 2.23 (s, 3H, CH$_3$), 7.22 (m, 2H), 7.66 (s, 1H), 11.34 (s, 1H, NH) ppm. HRMS-ESI m/z [M+H]$^+$ calcd for C$_{10}$H$_8$Cl$_3$N$_4$: 288.98091, found: 288.98086. Anal. Calcd for C$_{10}$H$_7$Cl$_3$N$_4$: C, 41.48; H, 2.44; N, 19.35. Found: C, 41.10; H, 2.53; N, 18.54.

4.2.2.4. (4-Chloro-phenyl)-(4,6-dichloro-[1,3,5]triazin-2-yl)-amine (98).
Prepared from commercially available 4-chloro-aniline (2.06 g, 16.2 mmol) and cyanuric chloride (3.0 g, 16.2 mmol) to yield **98** as white colored powder (3.4 g, 76%). Mp: 189–190 °C from acetone (lit. mp: 187–188 from benzene);[52] v_{max} (KBr disc) 3396, 1768, 1722, 1601, 1541 cm^{-1}, ^{1}H NMR (400 MHz, DMSO-d_6): δ 7.39 (m, 2H), 7.57 (m, 2H), 10.96 (br s, 1H, NH) ppm. ^{13}C NMR (100 MHz, DMSO-d_6,): δ 125.50 (2 × CH), 131.14 (2 × CH), 138.47 (C), 156.55 (C), 166.31 (C), 171.45 and 172.34 (C) ppm. HRMS-ESI m/z [M+H]$^+$ calcd for C$_9$H$_6$Cl$_3$N$_4$: 274.96526, found 274.96469. Anal. Calcd for C$_9$H$_5$Cl$_3$N$_4$: C, 39.23; H, 1.83; N, 20.33. Found: C, 39.64; H, 1.75; N, 20.11.

4.2.2.5. (4,6-Dichloro-[1,3,5]triazin-2-yl)-(4-nitro-phenyl)-amine (99).
Prepared from commercially available 4-nitro-aniline (3.8 g, 27.5 mmol) and cyanuric chloride (5 g, 27.3 mmol) to yield **99** as yellow powder (7.5 g, 95%). Mp: 288 °C from acetone (lit. mp: 290 from ethanol);[53] v_{max} (KBr disc) 3344, 1618, 1575, 1539 cm^{-1}, ^{1}H NMR (400 MHz, DMSO-d_6): δ 7.70 (m, 2H), 8.18 (m, 2H), and 10.94 (br s, 1H, NH) ppm. HRMS-ESI m/z [M−H]$^+$ calcd for C$_9$H$_4$Cl$_2$N$_5$O$_2$: 283.97475, found: 283.97475.

4.2.3. Preparation of 6-chloro-1,3,5-triazin-2,4-diamine derivatives (100–109, Scheme 2)
To a solution of the particular 4,6-dichloro-[1,3,5]triazin-2-yl)amine (**95–99**) in THF (50 ml) at 0 °C, diisopropylethylamine (acid scavenger, 2 equiv) and the selected alkylamine (2 equiv) were added sequentially. The resulting mixture was stirred at 0 °C for 30 min, then at room temperature for another 30 min before quenching with aqueous solution of ammonium chloride (50% w/v). Water/THF were totally removed in vacuo and the product was washed with water and purified by recrystallization from acetone/water.[45]

4.2.3.1. 6-Chloro-N-ethyl-N'-(2-methoxy-phenyl)-[1,3,5]triazine-2,4-diamine (100).
Prepared from **96** (2.25 g, 8.3 mmol) and ethylamine (0.75 g, 16.6 mmol) to yield **100** as cream-colored powder (1.84 g, 79%), mp: 178 °C from THF; v_{max} (KBr disc) 3387, 3261, 1626, 1575, 1518 cm^{-1}; ^{1}H NMR (400 MHz, DMSO-d_6, rotameric[45]): δ 1.10 (t, 3H), 3.2 (q, 2H), 3.80 (s, 3H, OCH$_3$), 6.91–7.1 (m, 4H), 7.3 (br d, 1H, NH) and 8.15 (br s, 1H, NH) ppm. HRMS-ESI m/z [M+H]$^+$ calcd for C$_{12}$H$_{15}$ClN$_5$O: 280.09596, found: 280.09544. Anal. Calcd for C$_{12}$H$_{14}$Cl$_1$N$_5$O: C, 51.52; H, 5.04; N, 25.04. Found: C, 51.23; H, 4.83; N, 24.45.

4.2.3.2. 6-Chloro-N-isopropyl-N'-(2-methoxy-phenyl)-[1,3,5]triazine-2,4-diamine (101).
Prepared from **96** (2 g, 7.3 mmol) and isopropylamine (0.86 g, 14.6 mmol) to yield **101** as off-white colored powder (4.5 g, 100%). Mp: 100 °C from THF; v_{max} (KBr disc) 3300, 1693, 1737 cm^{-1}; ^{1}H NMR (300 MHz, DMSO-d_6): 1.05 (d, 6H, 2 × CH$_3$), 3.93 (s, 3H, OMe), 4.02 (m, 1H), 7.02 (m, 3H), 7.70 (m, 1H), 7.90 (br s, 1H, NH), and 8.50 (s, 1H, NH) ppm. HRMS-ESI m/z [M+H]$^+$ calcd for C$_{13}$H$_{17}$ClN$_5$O: 294.11161, found: 294.11161. Anal. Calcd for C$_{13}$H$_{16}$ClN$_5$O: C, 53.15; H, 5.49; N, 23.84. Found: C, 53.34; H, 5.16; N, 23.92.

4.2.3.3. 6-Chloro-N-(2-methoxy-4-methyl-phenyl)-N'-pentyl-[1,3,5]triazine-2,4-diamine (102).
Prepared from **95** (2 g, 7 mmol) and pentylamine (1.2 g, 14 mmol) to yield **102** as white colored powder (2.3 g, 98%), mp 159–165 °C from THF. v_{max} (KBr disc) 3413, 3130, 1604, 1579. ^{1}H NMR (400 MHz, DMSO-d_6, rotameric[45]): δ 0.81 (m, 3H, CH$_3$), 1.24 (m, 4H, 2 × CH$_2$), 1.44 (m, 2H, CH$_2$), 2.23 (s, 3H, CH$_3$), 3.18 (m, 2H, CH$_2$), 3.75 (s, 3H, OCH$_3$), 6.88–6.93 (m, 3H), 7.53 (br s, exchangeable, NH), and 8.1 (br s, exchangeable, NH) ppm. ^{13}C NMR (100 MHz, DMSO-d_6, rotameric[45]): δ 16.54 (CH$_3$), 23.04 (CH$_2$), 24.44 (CH$_2$), 30.89 (CH$_2$), 31.11 (CH$_2$), 31.23 (CH$_3$), 58.43 (OCH$_3$), 113.78 (CH), 114.09 (CH), 127.73 (C), 128.85 (C), 131.43 (CH), 152.20 (C), 166.53 (C), 167.92 (C), and 170.52 (C) ppm. HRMS-ESI m/z [M+H]$^+$ calcd for C$_{16}$H$_{23}$ClN$_5$O: 336.15856, found: 336.15856; Anal. Calcd for C$_{16}$H$_{22}$ClN$_5$O: C, 57.22; H, 6.60; N, 20.85. Found: C, 56.49; H, 5.94; N, 20.11.

4.2.3.4. Chloro-N-isopropyl-N'-(2-methoxy-4-methyl-phenyl)-[1,3,5]triazine-2,4-diamine (103).
Prepared from **95** (1 g, 3.5 mmol) and isopropylamine (0.41 g, 7.0 mmol). to yield **103** as white powder (0.7, 65%). Mp: 145 °C from THF; v_{max} (KBr disc) 3396, 3256, 1581, 1493 cm^{-1}; ^{1}H NMR (400 MHz, DMSO-d_6, rotameric[45]): δ 1.20 (d, 6H, 2 × CH$_3$), 2.21 (s, 3H, CH$_3$), 3.04 (m, 1H), 3.71 (s, 3H, OMe), 6.83 (m, 3H), 7.64 (br s,1H, NH), and 7.95 (br s, 1H, NH) ppm. HRMS-ESI m/z [M+H]$^+$ calcd for C$_{14}$H$_{19}$ClN$_5$O: 308.12726, found: 308.12726.

4.2.3.5. 6-Chloro-N-(5-chloro-2-methyl-phenyl)-N'-ethyl-[1,3,5]triazine-2,4-diamine (104).
Prepared from **97** (1.0 g, 3.45 mmol) and ethylamine (0.31 g, 6.9 mmol) to yield **104** as rose colored powder (1.02 g, 99%). Mp: 182 °C from THF; v_{max} (KBr disc) 3433, 3297, 1626, 1574, 1529 cm^{-1}; ^{1}H NMR (400 MHz, DMSO-d_6, rotameric[45]): δ 1.05 (m, 3H, CH$_3$), 2.19 (s, 3H, CH$_3$), 3.20 (m, 2H, CH$_2$), 7.14–7.24 (m, 3H), 7.9 (br s, 1H, NH), and 9.4 (br s, 1H, NH) ppm. ^{13}C NMR (100 MHz, DMSO-d_6, rotameric[45]): δ 19.13 (CH$_3$), 22.29 (CH$_3$), 39.92 (CH$_2$), 129.5 (C), 130.27 (C), 134.48 (CH), 136.51 (CH), 142.46 (CH), 148.3 (C), 169.20 (C), 170.00 (C), and 172.95 (C). HRMS-ESI m/z [M+H]$^+$ calcd for C$_{12}$H$_{14}$Cl$_2$N$_5$: 298.06208, found: 298.06208.

4.2.3.6. 6-Chloro-N-(5-chloro-2-methyl-phenyl)-N'-pentyl-[1,3,5]triazine-2,4-diamine (105).

Prepared from **97** (1 g, 3.5 mmol) and pentylamine (0.6 g, 7 mmol) to yield **105** as pink powder (1.1 g, 91%), mp: 155 °C from THF; ν_{max} (KBr disc) 3427, 3265, 1624, 1568, 1518 cm^{-1}; ^{1}H NMR (400 MHz, DMSO-d_6, rotameric[45]): δ 0.83 (m, 3H, CH$_3$), 1.22 (m, 4H, 2 × CH$_2$), 1.45 (m, 2H, CH$_2$), 2.16 (m, 3H, CH$_3$), 3.13 (m, 2H, CH$_2$), 7.12–7.23 (m, 2H), 7.41 (m, 1H), 8.07 (br s, 1H, NH), and 9.40 (br s, 1H, NH) ppm. ^{13}C NMR (100 MHz, DMSO-d_6, rotameric[45]): δ 18.47 (CH$_3$), 22.27 (CH$_3$), 26.60 (CH$_2$), 33.23 (CH$_2$), 33.35 (CH$_2$), 39.99 (CH$_2$), 130.25 (C), 130.92 (C), 134.49 (CH), 136.47 (CH), 137.20 (C), 142.47 (CH), 169.19 (C), 170.16 (C), and 172.93 (C). HRMS-ESI m/z [M+H]$^+$ calcd for C$_{15}$H$_{20}$Cl$_2$N$_5$: 340.10903, found: 340.10903; Anal. Calcd for C$_{15}$H$_{19}$Cl$_2$N$_5$: C, 52.95; H, 5.63; N, 20.58. Found: C, 52.36; H, 5.48; N, 19.90.

4.2.3.7. 6-Chloro-N-(5-chloro-2-methyl-phenyl)-N'-isopropyl-[1,3,5]triazine-2,4-diamine (106).

Prepared from **97** (1.5 g, 5.2 mmol) and isopropylamine (0.61 g, 10.4 mmol). to yield **106** as rose powder (1.3 g, 80%), mp: 220 °C; ν_{max} (KBr disc) 3234, 2976, 1597, 1531 cm^{-1}; ^{1}H NMR (400 MHz, DMSO-d_6, rotameric[45]): δ 1.09 (d, 6H, 2 × CH$_3$), 2.16 (s, 3H, 3 × CH$_3$), 3.90 (m, 1H, CH), 7.09–7.22 (m, 2H), 7.41–7.60 (m, 1H), 7.78 (d,1H, NH), and 9.28 (br s,1H, NH) ppm. ^{13}C NMR (100 MHz, DMSO-d_6, rotameric[45]): δ 22.26 (CH$_3$), 26.98 (CH$_3$), 46.91 (CH), 129.57 (C), 130.98 (C), 134.51 (CH), 136.41 (CH), 137.2 (C), 142.48 (CH), 169.29 (C), 172.99 (C), and 173.60 (C) ppm. HRMS-ESI m/z [M+H]$^+$ calcd for C$_{13}$H$_{16}$Cl$_2$N$_5$: 312.07773, found: 312.07740.

4.2.3.8. 6-Chloro-N-(4-chloro-phenyl)-N'-ethyl-[1,3,5]triazine-2,4-diamine (107)[55].

Prepared from **98** (1.0 g, 3.63 mmol) and ethylamine (0.32 g, 7.2 mmol) to yield **107** as white powder (0.97 g, 94%), mp: 220–222 °C from THF; ν_{max} (KBr disc) 3259, 1637, 1579, 1527 cm^{-1}; ^{1}H NMR (400 MHz, DMSO-d_6, rotameric[45]): δ 1.13 (m, 3H, CH$_3$), 3.25 (m, 2H, CH$_2$), 7.3–7.4 (m, 2H, 2 × CH), 7.72–7.82 (m, 2H, 2 × CH), 8.10 (br s, 1H, NH), and 8.30 (br s, 1H, NH) ppm. ^{13}C NMR (100 MHz, DMSO-d_6, rotameric[45]): δ 16.77 (CH$_3$), 37.82 (CH$_2$), 124.15 (2 × CH), 128.80 (C), 131.1 (2 × CH), 140.64 (C), 166.20 (C), 167.80 (C), and 170.10 (C) ppm; HRMS-ESI m/z [M+Na]$^+$ calcd for C$_{11}$H$_{11}$Cl$_2$N$_5$Na: 306.02837, found: 306.02823; Anal. Calcd for C$_{11}$H$_{11}$Cl$_2$N$_5$: C, 46.50; H, 3.90; N, 24.65. Found: C, 46.04; H, 4.12; N, 23.28.

4.2.3.9. 6-Chloro-N-(4-chloro-phenyl)-N'-pentyl-[1,3,5]triazine-2,4-diamine (108).

Prepared from **98** (1.0 g, 3.63 mmol) and pentylamine (0.63 g, 7.2 mmol) to yield **108** as white powder (1.1 g, 94%). Mp 190–192 °C from THF; ν_{max} (KBr disc) 3265, 3119, 1639, 1579 cm^{-1}; ^{1}H NMR (400 MHz, DMSO-d_6, rotameric[45]): δ 0.82 (m, 3H, CH$_3$), 1.28 (m, 4H, 2 × CH$_2$), 1.49 (m, 2H, CH$_2$), 3.23 (m, 2H, CH$_2$), 7.30 (m, 2H, 2 × CH), 7.71 (m, 2H, 2 × CH), 8.21 (br s,1H, NH), 10.14 (br s,1H, NH) ppm.. ^{13}C NMR (100 MHz, DMSO-d_6): δ 16.5 (CH$_3$), 24.8 (CH$_2$), 30.83 (CH$_2$), 31.12 (CH$_2$), 43.18 (CH$_2$), 124.11 (2 × CH), 129.02 (C), 130.99 (2 × CH), 140.66 (C), 166.29 (C), 167.99 (C), and 170.49 (C) ppm; HRMS-ESI m/z [M+H]$^+$ calcd for C$_{14}$H$_{18}$Cl$_2$N$_5$: 326.09338, found: 326.09338; Anal. Calcd for C$_{14}$H$_{17}$Cl$_2$N$_5$: C, 51.54; H, 5.25; N, 21.47. Found: C, 51.16; H, 4.74; N, 20.57.

4.2.3.10. 6-Chloro-N-(4-nitro-phenyl)-N'-pentyl-[1,3,5]triazine-2,4-diamine (109).

Prepared from **99** (2 g, 7.0 mmol) and pentylamine (1.2 g, 13.7 mmol) to yield **109** as yellow powder (1.95 g, 83%). Mp 188–193 °C from THF; ν_{max} (KBr disc) 3300, 1635, 1541 cm^{-1}; ^{1}H NMR (400 MHz, DMSO-d_6, rotameric[45]): δ 0.84 (m, 3H, CH$_3$), 1.29 (m, 4H, 2 × CH$_2$), 1.54 (m, 2H, CH$_2$), 3.33

(m, 2H, CH$_2$), 7.93–8.10 (m, 2H) 8.13–8.17 (m, 2H), 8.39 (br s, 1H, NH), and 10.55 (br s, 1H, NH) ppm. ^{13}C NMR (100 MHz, DMSO-d_6): δ 16.56 (CH$_3$), 24.51 (CH$_2$), 30.75 (CH$_2$), 31.26 (CH$_2$), 43.32 (CH$_2$), 124.84 (2 × CH), 127.28 (2 × CH), 144.16 (C), 148.27 (C), 166.40 (C), 167.95 (C), and 170.61 (C) ppm; HRMS-ESI m/z [M−H]$^+$ calcd for C$_{14}$H$_{16}$ClN$_6$O$_2$: 335.10287, found: 335.10288.

4.2.4. Preparation of 4-[4-alkylamino-6-(phenylamino)-[1,3,5]triazin-2-yl]-piperazine-1-carboxylic acid *tert*-butyl ester derivatives (110–111, Scheme 3)

To a solution of the particular monochlorotriazine derivative (**100**, **105**) in dioxane (50 ml) 1-N-Boc-piperazine (ca. 1.5 equiv) and diisopropylethylamine (acid scavenger, 2 equiv) were added successively. The reaction subsequently refluxed until completion as revealed by TLC. Distilled water (20 ml) was added to the reaction mixture and the resulting suspension was left at 4 °C over few days. The resulting suspensions were filtered and the solid residues were further purified by recrystallization from acetone/water (Scheme 3).[45]

4.2.4.1. 4-[4-Ethylamino-6-(2-methoxy-phenylamino)-[1,3,5]triazin-2-yl]-piperazine-1-carboxylic acid *tert*-butyl ester (110).

Prepared from **100** (0.7 g, 2.5 mmol) and 1-N-Boc-piperazine (0.69 g, 3.70 mmol) to yield **110** as white powder (0.75 g, 70%), mp 161–162 from acetone/water; ν_{max} (KBr disc) 3433, 3290, 2976, 1693 and 1575 cm^{-1}. ^{1}H NMR (400 MHz, DMSO-d_6): δ 1.08 (t, 3H, CH$_3$, J = 7.16), 1.42 (s, 9H, 3 × CH$_3$), 3.26 (m, 2H, CH$_2$), 3.34 (br s, 4H, 2 × CH$_2$), 3.68 (br s, 4H, 2 × CH$_2$), 3.86 (s, 3H, OCH$_3$), 6.9–7.1 (m, 4H), 7.30–7.40 (br s, 1H, NH), and 8.28–8.29 (br s, 1H, NH) ppm; ^{13}C NMR (100 MHz, DMSO-d_6, rotameric[45]): δ 14.80 (CH$_3$), 28.03 (3 × CH$_3$), 34.82 (CH$_2$), 42.44 (2 × CH$_2$), 55.70 (OCH$_3$), 66.32 (2 × CH$_2$), 78.99 (C), 110.52 (CH) 119.76 (CH), 120.34 (CH), 121.99 (CH), 128.61 (C), 148.14 (C), 153.87 (C=O), 163.76 (C), 164.49 (C), and 165.35 (C) ppm. HRMS-ESI m/z [M+H]$^+$ calcd for C$_{21}$H$_{32}$N$_7$O$_3$: 430.25611, found: 430.25493.

4.2.4.2. 4-[4-(5-Chloro-2-methyl-phenylamino)-6-pentylamino-[1,3,5]triazin-2-yl]-piperazine-1-carboxylic acid *tert*-butyl ester (111).

Prepared from **105** (0.5 g, 1.47 mmol) and 1-N-Boc-piperazine (0.27 g, 1.47 mmol) to yield **111** as brown powder (0.61 g, 85%), mp: 123–124 from acetone/water; ν_{max} (KBr disc) 3447, 3364, 1682, 1606, 1545 cm^{-1}. ^{1}H NMR (400 MHz, DMSO-d_6, rotameric[45]): δ 0.84 (m, 3H, CH$_3$), 1.26 (m, 4H, 2 × CH$_2$), 1.42 (s, 9H, 3 × CH$_3$), 1.46 (m, 2H, CH$_2$), 2.18 (s, 3H, CH$_3$, splitted due to rotamers), 3.17 (m, 2H, CH$_2$), 3.21 (m, 4H, 2 × CH2), 3.65 (m, 4H, 2 × CH$_2$), 6.89–7.18 (m, 3H, 3 × CH), 7.62 (br s, 1H, NH), and 8.15 (br s, 1H, NH) ppm;^{13}C NMR (100 MHz, DMSO-d_6 rotameric[45]): δ 13.91 (CH$_3$), 17.51 (CH$_3$), 21.85 (CH$_2$), 28.01 (3 × CH$_3$), 28.61 (2 × CH$_2$), 28.75 (CH$_2$), 29.11 (CH$_2$), 39.85 (CH$_2$), 42.32 (2 × CH$_2$), 78.99 (C), 122.78 (CH), 123.73 (CH), 129.21 (C), 129.56 (C), 131.26 (CH), 139.12 (C), 153.87 (C=O), 164.38 (C), 164.50 (C), and 165.66 (C) ppm. HRMS-ESI m/z [M+H]$^+$ calcd for C$_{24}$H$_{37}$ClN$_7$O$_2$: 490.26918, found: 490.26949.

4.2.5. 4-[4-Alkylamino-6-(phenylamino)-[1,3,5]triazin-2-yl]-piperazin-1-ium; chloride derivatives (112–113, Scheme 3)

The particular N-protected-piperazinyl-triazine derivative (**110**, **111**) was dissolved in methanol (25 ml) and magentically stirred at 0 °C for 30 min. Subsequently, aqueous HCl solution (6 ml, 6 N) was added dropwise to the methanolic solution at 0 °C over 70 min. Thereafter, the resulting mixture was warmed to ambient temperature over 3 h, then was slowly heated to an internal temperature of 50 °C and left on a stirrer for 24 h. The resulting aqueous solution was cooled to 0 °C and made alkaline (pH 14) by addition NaOH solution (10% w/v). The resulting alkaline solution

was extracted with chloroform (3 × 25 ml) and the organic phases were combined and dried over magnesium sulfate. The solvent is left to evaporate in vacuo to afford the yellow oil. Finally, the oil was dissolved in acetone (10 ml), filtered and, then precipitated by acetonic HCl to yield the final product as white powder.

4.2.5.1. N-Ethyl-N′-(2-methoxy-phenyl)-6-piperazin-1-yl-[1,3,5]triazine-2,4-diamine·HCl (112).
Prepared from compound **110** (0.5 g, 1.17 mmol) to yield **112** as white powder (0.40 g, 78%), mp: 256 (Decomp.); v_{max} (KBr disc) 3431, 1639, 1595 cm^{-1}; ^{1}H NMR (300 MHz, DMSO-d_6, as rotameric[45]): ^{1}H NMR (300 MHz, DMSO-d_6): δ 1.10 (t, 3H, CH$_3$, J = 7.0), 3.10 (m, 4H, 2 × CH$_2$), 3.31 (m, 2H, CH$_2$), 3.79 (s, 3H, OCH$_3$), 3.96 (m, 4H, 2 × CH$_2$), 6.92–7.19 (m, 3H), 7.74 (m, 1H), 8.76 (br s, 1H, NH), 9.70 (br s, 1H, NH), and 9.90 (br s, 1H, NH) ppm. ^{13}C NMR (75 MHz, DMSO-d_6, appears as two rotamers): δ 14.60 (CH$_3$), 35.85 (CH$_2$), 40.97 (2 × CH$_2$), 42.47 (2 × CH$_2$) 56.32 (OCH$_3$), 112.00 (CH), 120.86 (CH), 123.21 (CH), 124.63 (C), 125.94 (CH), 126.88 (C), 150.84 (C), 155.02 (C) and 162 (br, C) ppm. HRMS-ESI m/z [M+H]$^+$ calcd for C$_{16}$H$_{24}$N$_7$O: 330.20368, found 330.20247; Anal. Calcd for C$_{16}$H$_{23}$N$_7$O·3HCl: C, 43.80; H, 5.97; N, 22.35. Found: C, 42.45; H, 5.61; N, 21.57.

4.2.5.2. 4-[4-(5-Chloro-2-methyl-phenylamino)-6-pentylamino-[1,3,5]triazin-2-yl]-piperazine·HCl (113).
Prepared from **111** (0.5 g, 1.02 mmol) to yield **113** as white powder (0.3 g, 57%), mp 124 °C from acetone (Decomp.); v_{max} (KBr disc) 3421, 1602, 1572, 1548 cm^{-1}; ^{1}H NMR (400 MHz, DMSO-d_6, rotameric[45]): δ 0.84 (m, 3H, CH$_3$), 1.23 (m, 4H, 2 × CH$_2$), 1.46 (m, 2H, CH$_2$), 2.18 (s, 3H, CH$_3$, splitted due to rotamers), 3.18 (m, 2H, CH$_2$), 3.69 (m, 4H, 2 × CH$_2$), 6.87–7.18 (m, 3H), 7.63 (br s, 1H, NH), and 8.11 (br s, 1H, NH) ppm; ^{13}C NMR (100 MHz, DMSO-d_6, rotameric[45]): δ 13.92 (CH$_3$), 17.52 (CH$_3$), 21.84 (CH$_2$), 28.60 (CH$_2$), 29.11 (CH$_2$), 39.72 (CH$_2$), 42.34 (2 × CH$_2$), 44.43 (2 × CH$_2$), 122.73 (CH), 123.67 (CH), 129.54 (C), 130.10 (C), 131.29 (CH) 139.25 (C), 164.37 (2 × C), and 165.7 (C) ppm. HRMS-ESI m/z [M+H]$^+$ calcd for C$_{19}$H$_{29}$ClN$_7$: 390.21675, found: 390.21675. Anal. Calcd for C$_{19}$H$_{28}$ClN$_7$·H$_2$O·3HCl: C, 44.11; H, 6.43; N, 18.95. Found: C, 43.37; H, 6.20; N, 17.85.

4.2.6. Preparation of 6-[4-(2-dimethylamino-ethyl)-piperazin-1-yl]-N-(phenyl)-N′-alkyl-[1,3,5]triazine-2,4-diamine (114–123, Scheme 4)

To a magnetically stirred solution of the particular monochloro-diamino-triazine derivative (**100–109**) in THF (20 ml), 1-[2-(dimethylamino)ethyl]piperazine (1.5–3 equiv) and triethylamine (acid scavenger, 2 equiv) were added sequentially. The resulting mixture was stirred at room temperature until completion as revealed by TLC (roughly over two days). Subsequently, the reaction mixture was filtred and the filtrate was dried in vacuo. The residue was dissolved in acetone, filtered and precipitated by acetonic HCl to yield powdered product (Scheme 4).[63]

4.2.6.1. 6-[4-(2-Dimethylamino-ethyl)-piperazin-1-yl]-N-ethyl-N′-(2-methoxy-phenyl)-[1,3,5]triazine-2,4-diamine (114).
Prepared from **100** (0.40 g, 1.43 mmol) and 1-[2-(dimethyl amino) ethyl] piperazine (0.36 g, 2.29 mmol) and triethylamine (0.29 g, 2.87 mmol) to yield **114** as white powder (0.4 g, 48%), mp: 230 °C (Decomp.) from acetone; v_{max} (KBr disc) 3421, 1620, 1593, 1547 cm^{-1}; ^{1}H NMR (400 MHz, DMSO-d_6, rotameric[45], protonated sample): δ 1.14 (m, 3H, CH$_3$), 2.83 (s, 6H, N(CH$_3$)$_2$), 3.04 (m, 2H, CH$_2$), 3.19 (m, 4H, 2 × CH$_2$), 3.62 (s, 3H, OCH$_3$), 3.83 (m, 8H, 4 × CH$_2$), 6.99–7.89 (m, 4H), 8.92 (br s, 1H, NH), and 10.07 (br s, 1H, NH) ppm; ^{13}C NMR (100 MHz, DMSO-d_6): δ 14.03 (CH$_3$), 35.37 (CH$_2$), 42.33 (N(CH$_3$)$_2$), 49.33 (CH$_2$), 50.29 (CH$_2$), 52.75

(2 × CH$_2$), 55.81 (OCH$_3$), 57.90 (2 × CH$_2$), 111.70 (br s, 2 × CH), 120.4 (br s, 2 × CH), 122.0 (br s, C) 126.0 (br s, C), 152.0 (br s, C), 156 (br s, C), and 161.0 (br s, C) ppm. HRMS-ESI m/z [M+H]$^+$ calcd for C$_{20}$H$_{33}$N$_8$O: 401.27718, found: 401.27718. Anal. Calcd for C$_{20}$H$_{32}$N$_8$O·5HCl: C, 41.22; H, 6.40; N, 19.23. Found: C, 41.74; H, 6.22; N, 19.03.

4.2.6.2. 6-[4-(2-Dimethylamino-ethyl)-piperazin-1-yl]-N-isopropyl-N′-(2-methoxy-phenyl)-[1,3,5]triazine-2,4-diamine (115).
Prepared from **101** (0.50 g, 1.7 mmol) and 1-[2-(dimethylamino)ethyl] piperazine (0.35 g, 2.23 mmol) and triethylamine (0.29 g, 2.9 mmol) to yield **115** as brown powder (0.62 g, 56%), mp: 240 (Decomp.) from acetone; v_{max} (KBr disc) 3491, 1643, 1531 cm^{-1}; ^{1}H NMR (400 MHz, DMSO-d_6 and TFA-d, rotameric[45], protonated sample): δ 1.1 (d, 6H, 2 × CH$_3$), 2.86 (s, 6H, N(CH$_3$)$_2$), 3.49–3.61 (m, 12H, 6 × CH$_2$), 3.83 (s, 3H, OCH$_3$), 4.14 (m, 1H, CH), 6.98–7.89 (m, 4H), 9.10 (br s, 1H, NH, d-Exchangeable), 10.0 (br s, 1H, NH, d-Exchangeable) ppm; ^{13}C NMR (100 MHz, DMSO-d_6, rotameric[45]): δ 21.45 (2 × CH$_3$), 39.82 (CH$_2$), 42.30 (N(CH$_3$)$_2$), 42.80 (CH), 48.26 (CH$_2$), 49.60 (2 × CH$_2$), 49.68 (2 × CH$_2$), 55.59 (OCH$_3$), 111.38 (CH), 111.84 (CH), 113.45 (C), 116.31 (C), 120.42 (CH), 125.70 (CH), 157.63 (C), 158.02 (C), and 158.40 (C) ppm. HRMS-ESI m/z [M+H]$^+$ calcd for C$_{21}$H$_{35}$N$_8$O: 415.29283, found: 415.29192. Anal. Calcd for C$_{21}$H$_{34}$N$_8$O·5H$_2$O·4HCl: C, 38.78; H, 7.44; N, 17.23. Found: C, 37.86; H, 7.03; N, 16.51.

4.2.6.3. N-(5-Chloro-2-methyl-phenyl)-6-[4-(2-dimethylamino-ethyl)-piperazin-1-yl]-N′-ethyl-[1,3,5]triazine-2,4-diamine (116).
Prepared from **104** (0.40 g, 1.34 mmol) and 1-[2-(dimethylamino)ethyl] piperazine (0.317 g, 2.02 mmol) and triethylamine (0.27 g, 2.6 mmol) to yield **116** as white powder (0.278 g, 39%), mp 240 °C (Decomp.) from acetone; v_{max} (KBr disc) 3649, 3800, 1655, 1624 cm^{-1}; ^{1}H NMR (300 MHz, DMSO-d_6, rotameric,[45] protonated sample): δ 1.07 (t, 3H, CH$_3$, J = 7), 2.21 (s, 3H, CH$_3$), 2.79 (s, 6H, N(CH$_3$)$_2$), 3.34 (m, 8H, 4 × CH$_2$), 3.58 (m, 6H, 3 × CH$_2$), 7.24–7.73 (m, 3H), 8.80 (br s, 1H, NH), and 10.30 (br s, 1H, NH) ppm; ^{13}C NMR (75 MHz, DMSO-d_6, rotameric[45]): δ 14.57 (CH$_3$), 18.06 (CH$_3$), 35.87 (CH$_2$), 42.75 (2 × CH$_3$, N(CH$_3$)$_2$), 49.79 (2 × CH$_2$), 50.25 (2 × CH$_2$), 50.77 (br s, 2 × CH$_2$), 124.56 (CH), 125.54 (CH), 130.58 (C), 131.90 (C), 132.44 (CH), 136.07 (C), 155.65 (C), 160.0 (C) and 161.55 (C) ppm. HRMS-ESI m/z [M+H]$^+$ calcd for C$_{20}$H$_{32}$ClN$_8$: 419.24330, found: 419.24301. Anal. Calcd for C$_{20}$H$_{31}$ClN$_8$·3HCl: C, 45.46; H, 6.49; N, 21.21. Found: C, 44.92; H, 6.49; N, 20.30.

4.2.6.4. N-(5-Chloro-2-methyl-phenyl)-6-[4-(2-dimethylamino-ethyl)-piperazin-1-yl]-N′-pentyl-[1,3,5]triazine-2,4-diamine (117).
Prepared from **105** (0.40 g, 1.18 mmol) and 1-[2-(dimethylamino)ethyl] piperazine (0.45 g, 2.9 mmol) and triethylamine (0.24 g, 2.37 mmol) to yield **117** as white powder (0.067 g, 9%), mp 71–72 °C from acetone (unprotonated sample); v_{max} (KBr disc) 3431, 1577, 1543, 1500 cm^{-1}; ^{1}H NMR (400 MHz, DMSO-d_6, rotameric,[45] unprotonated sample): δ 0.84 (m, 3H, CH$_3$), 1.23 (m, 4H, 2 × CH$_2$), 1.46 (m, 2H, CH$_2$), 2.13 (s, 6H, N(CH$_3$)$_2$), 2.34 (s, 3H, CH$_3$), 2.38 (m, 8H, 4 × CH$_2$), 3.19 (m, 2H, CH$_2$), 3.64 (m, 4H, 2 × CH$_2$), 6.83–7.18 (m, 3H) 7.65 (br s, 1H, NH), and 8.07 (br s, 1H, NH) ppm; ^{13}C NMR (100 MHz, DMSO-d_6, rotameric[45]): δ 13.92 (CH$_3$), 17.51 (CH$_3$), 21.83 (CH$_2$), 28.61 (CH$_2$), 29.14 (CH$_2$), 39.53 (CH$_2$), 42.55 (CH$_2$), 45.51 (2 × CH$_3$, N(CH$_3$)$_2$), 52.93 (2 × CH$_2$) 55.90 (CH$_2$), 56.58 (2 × CH$_2$), 122.66 (CH), 123.59 (CH), 129.06 (C), 129.54 (C), 131.28 (CH), 139.27 (C), 164.36 (C), 1 64.50 (C), and 165.77 (C) ppm. HRMS-ESI m/z [M+H]$^+$ calcd for C$_{23}$H$_{38}$ClN$_8$: 461.29025, found: 461.29033. Anal. Calcd for C$_{23}$H$_{37}$ClN$_8$·5HCl: C, 42.94. Found: C, 41.49.

4.2.6.5. N-(5-Chloro-2-methyl-phenyl)-6-[4-(2-dimethylamino-ethyl)-piperazin-1-yl]-N'-isopropyl-[1,3,5]triazine-2,4-diamine (118).

Prepared from **106** (0.50 g, 1.6 mmol) and 1-[2-(dimethylamino)ethyl] piperazine (0.38 g, 2.42 mmol) and triethylamine (0.32 g, 3.17 mmol) to yield **118** as white powder (0.44 g, 46%), mp: 245 °C (Decomp.) from acetone; v_{max} (KBr disc) 3447, 1655, 1626, 1593 cm^{-1}, ^{1}H NMR (400 MHz, DMSO-d_6, rotameric,[45] protonated sample): δ 1.18 (d, 6H, 2 × CH$_3$, J = 8), 2.24 (s, 3H, CH$_3$), 2.82 (s, 6H, N(CH$_3$)$_2$), 3.43 (m, 12H, 6 × CH$_2$), 4.14 (m, 1H, CH), 7.24–7.28 (m, 3H), 7.59 (br s, H, NH), and 8.10 (br, s, H, NH) ppm. HRMS-ESI m/z [M+H]$^+$ calcd for C$_{21}$H$_{34}$ClN$_8$: 433.25895, found: 433.25228; Anal. Calcd for C$_{21}$H$_{33}$ClN$_8$·4HCl·H$_2$O: C, 42.26; H, 6.59; N, 18.77. Found: C, 42.15; H, 6.41; N, 18.33.

4.2.6.6. 6-[4-(2-Dimethylamino-ethyl)-piperazin-1-yl]-N-isopropyl-N'-(2-methoxy-4-methyl-phenyl)-[1,3,5]triazine-2,4-diamine (119).

Prepared from **103** (0.4 g, 1.30 mmol) and 1-[2-(dimethylamino)ethyl] piperazine (0.53 g, 3.37 mmol) and triethylamine (0.23 g, 2.27 mmol) to yield **119** as white powder (0.22 g, 28%), mp: 214 °C (Decomp.) from acetone; v_{max} (KBr disc) 3435, 1629, 1599, 1535 cm^{-1}, ^{1}H NMR (300 MHz, DMSO-d_6, rotameric,[45] protonated sample): δ 1.20 (d, 6H, 2 × CH$_3$), 2.21 (s, 3H, CH$_3$), 2.79 (s, 6H, N(CH$_3$)$_2$), 3.56–3.75 (m, 12H, 6 × CH$_2$), 3.71 (s, 3H, OMe), 4.10 (m, 1H), 6.92 (m, 3H), 7.48 (br s,1H, NH), and 8.70 (br s, 1H, NH) ppm. ^{13}C NMR (75 MHz, DMSO-d_6, rotameric[45]): δ 20.82 (CH$_3$) 22.34 (2 × CH$_3$), 41.05 (CH$_2$), 42.81 (2 × CH$_3$, N(CH$_3$)$_2$), 43.33 (CH), 49.94 (CH$_2$), 50.41 (2 × CH$_2$) 50.91 (2 × CH$_2$), 56.36 (OCH$_3$), 111.83 (CH), 123.85 (CH), 125.94 (CH), 127.50 (C), 129.50 (C), 148.79 (C), 150.0 (C), 155.46 (C), and 162.50 (C) ppm. HRMS-ESI m/z [M+H]$^+$ calcd for C$_{22}$H$_{37}$N$_8$O: 429.30848, found: 429.30848. Anal. Calcd for C$_{22}$H$_{37}$ClN$_8$O·5HCl: C, 43.25; H, 6.76; N, 18.34. Found: C, 44.14; H, 6.82; N, 18.37.

4.2.6.7. 6-[4-(2-Dimethylamino-ethyl)-piperazin-1-yl]-N-(2-methoxy-4-methyl-phenyl)-N'-pentyl-[1,3,5]triazine-2,4-diamine (120).

Prepared from **102** (0.5 g, 1.5 mmol) and 1-[2-(dimethylamino)ethyl] piperazine (0.69 g, 4.4 mmol) and diisopropylethylamine (0.34 g, 2.6 mmol) to yield **120** as cream colored powder (0.44 g, 64%). Mp: 240 (Decomp.) from acetone; v_{max} (KBr disc) 3425, 1616, 1506 cm^{-1}, ^{1}H NMR (400 MHz, DMSO-d_6, rotameric,[45] unprotonated sample): δ 0.85 (m, 3H, CH$_3$), 1.29 (m, 4H, 2 × CH$_2$), 1.51 (m, 2H, CH$_2$), 2.24 (s, 6H, N(CH$_3$)$_2$), 2.25 (s, 3H, CH$_3$), 2.36 (m, 8H, 4 × CH$_2$), 3.24 (m, 2H, CH$_2$), 3.60 (m, 4H, 2 × CH$_2$), 3.81 (s, 3H, OCH$_3$), 6.73–7.03 (m, 3H), 7.30 (br s, 1H, NH) and 8.21 (br s, 1H, NH) ppm; ^{13}C NMR (100 MHz, DMSO-d_6, rotameric[45]): δ 13.90, (CH$_3$), 20.73 (CH$_3$), 21.84 (CH$_2$), 28.64 (CH$_2$), 29.01 (CH$_2$), 39.52 (CH$_2$), 42.64 (CH$_2$), 45.49 (N(CH$_3$)$_2$), 52.91 (2 × CH$_2$), 55.73 (OCH$_3$), 55.90 (CH$_2$), 56.57 (2 × CH$_2$), 110.23 (CH), 120.29 (CH), 121.79 (CH), 128.40 (C) 128.77 (C), 145.80 (C), 163.70 (C), 164.32 (C) and 165.56 (C) ppm. HRMS-ESI m/z [M+Na]$^+$ calcd for C$_{24}$H$_{40}$N$_8$NaO: 479.32173, found: 479.32172.

4.2.6.8. N-(4-Chloro-phenyl)-6-[4-(2-dimethylamino-ethyl)-piperazin-1-yl]-N'-ethyl-[1,3,5]triazine-2,4-diamine (121).

Prepared from **107** (0.4 g, 1.41 mmol) and 1-[2-(dimethylamino)ethyl] piperazine (0.66 g, 4.2 mmol) and triethylamine (0.28 g, 2.8 mmol) to yield **121** as white powder (0.3 g, 52%). Mp: 232 (Decomp.) from acetone. v_{max} (KBr disc) 3437, 1624, 1591 cm^{-1}, ^{1}H NMR (400 MHz, DMSO-d_6, rotameric,[45] unprotonated sample): δ 1.05 (t, 3H, CH$_3$, J = 8), 2.10 (s, 6H, N(CH$_3$)$_2$), 2.35 (m, 8H, 4 × CH$_2$), 3.25 (m, 2H, CH$_2$), 3.60 (m, 4H, 2 × CH$_2$), 6.84 (br s, 1H, NH), 7.28 (m, 2H) 7.71 (m, 2H), and 8.94

(br s, 1H, NH) ppm; ^{13}C NMR (100 MHz, DMSO-d_6, rotameric[45]): δ 17.50 (CH$_3$), 37.45 (CH$_2$), 45.28 (2 × CH$_3$, N(CH$_3$)$_2$), 48.07 (2 × CH$_2$), 55.55 (2 × CH$_2$), 58.39 (CH$_2$), 59.02 (CH$_2$), 123.46 (2 × CH), 127.50 (C), 130.76 (2 × CH), 142.20, 166.20 (C), 167.00 (C), and 167.80 (C) ppm. HRMS-ESI m/z [M+H]$^+$ calcd for C$_{19}$H$_{30}$ClN$_8$: 405.22765, found: 405.22778. Anal. Calcd for C$_{19}$H$_{29}$ClN$_8$·5HCl: C, 38.86; H, 5.84; N, 19.08. Found: C, 39.67; H, 5.58; N, 19.14.

4.2.6.9. N-(4-Chloro-phenyl)-6-[4-(2-dimethylamino-ethyl)-piperazin-1-yl]-N'-pentyl-[1,3,5]triazine-2,4-diamine (122).

Prepared from **108** (0.4 g, 1.2 mmol) 1-[2-(dimethylamino)ethyl] piperazine (0.56 g, 3.6 mmol) and diisopropylethylamine (0.05 g, 0.38 mmol) to yield **122** as off-white powder (0.24 g, 31%). Mp: 224 °C (Decomp.) from acetone. v_{max} (KBr disc) 3425, 1616, 1506 cm^{-1}, ^{1}H NMR (400 MHz, DMSO-d_6, rotameric[45], protonated sample): δ 0.87 (m, 3H, CH$_3$), 1.30 (m, 4H, 2 × CH$_2$), 1.53 (m, 2H, CH$_2$), 2.83 (s, 6H, N(CH$_3$)$_2$), 3.33 (m, 2H,CH$_2$), 3.60–3.79 (m, 12, 6 × CH$_2$), 7.39 (m, 2H), 7.64 (m, 2H), 8.30 (br s, 1H, NH) and 11.0 (br s, 1H, NH) ppm; ^{13}C NMR (100 MHz, DMSO-d_6): δ 13.89 (CH$_3$), 21.75 (CH$_2$), 28.20 (CH$_2$), 28.39 (CH$_2$), 40.47 (CH$_2$), 42.38 (N(CH$_3$)$_2$), 49.51 (2 × CH$_2$), 49.9 (2 × CH$_2$), 50.50 (CH$_2$), 50.56 (CH$_2$), 122.02 (2 × CH), 124.11 (C), 128.68 (2 × C), 140.60 (C), 155.34 (C), 156.82 (C), and 164.04 (C) ppm. HRMS-ESI m/z [M+H]$^+$ calcd for C$_{22}$H$_{36}$ClN$_8$: 447.27460, found: 447.27430. Anal. Calcd for C$_{22}$H$_{35}$ClN$_8$·5HCl: C, 41.99; H, 6.41; N, 17.81. Found: C, 41.82; H, 6.37; N, 17.32.

4.2.6.10. 6-[4-(2-Dimethylamino-ethyl)-piperazin-1-yl]-N-(4-nitro-phenyl)-N'-pentyl-[1,3,5]triazine-2,4-diamine (123).

Prepared from **109** (0.4 g, 1.19 mmol) and 1-[2-(dimethylamino)ethyl] piperazine (0.56 g, 3.56 mmol) and diisopropylethylamine (0.05 g, 0.38 mmol) to yield **123** as off-white powder (0.4 g, 51%). Mp: 237 °C (Decomp.) from acetone; v_{max} (KBr disc) 3464, 1662, 1626, 1585 cm^{-1}; ^{1}H NMR (300 MHz, DMSO-d_6, rotameric[45], protonated sample): δ 0.84 (m, 3H. CH$_3$), 1.28 (m, 4H, 2 × CH$_2$), 1.51 (m, 2H, CH$_2$), 2.81 (s, 6H, N(CH$_3$)$_2$), 3.57 (m, 4H, 2 × CH$_2$), 3.96 (m, 10H, 5 × CH$_2$), 7.93 (d, 2H, J = 9.0), 7.68 (br s, 1H, NH), 8.12 (d, 2H, J = 9.0), and 10.22 (br s, 1H, NH) ppm; ^{13}C NMR (75 MHz, DMSO-d_6): δ 14.40 (CH$_3$), 22.32 (CH$_2$), 29.07 (2 × CH$_2$), 40.77 (CH$_2$), 42.93 (N(CH$_3$)$_2$), 50.15 (2 × CH$_2$), 50.61 (2 × CH$_2$), 51.24 (2 × CH$_2$), 119.63 (2 × CH), 125.21 (2 × CH), 141.64 (C), 146.81 (C), 163.21 (C), 163.78 (C) and 164.20 (C) ppm. HRMS-ESI m/z [M+H]$^+$ calcd for C$_{22}$H$_{36}$N$_9$O$_2$: 458.29865, found: 458.29756. Anal. Calcd for C$_{22}$H$_{35}$N$_9$O$_2$·3H$_2$O·4HCl: C, 40.19; H, 6.90; N, 19.17. Found: C, 40.14; H, 6.73; N, 18.11.

4.3. In vitro experimental studies

4.3.1. Materials

All of the chemicals used in these experiments were of reagent grade and obtained from commercial suppliers. NCI samples were kindly provided by the National Cancer Institute. CaMKII drug discovery kit was purchased from Cyclex (Japan), the standard inhibitor KN-62, water and DMSO for bioanalysis were all purchased form Sigma–Aldrich (USA).

4.3.2. Preparation of hit compounds for In vitro assay

The tested compounds were provided as dry powders in variable quantities (5 mg to 10 mg). They were initially dissolved in DMSO to give stock solutions of fixed concentrations. Subsequently, they were diluted to the required concentrations with deionized water for bioassay.

4.3.3. Quantification of CaMKII activity in a spectrophotometric assay

The activity of the in silico hits were quantified by CaMKII drug discovery kit (Cyclex, Japan). The 96-well plate of the kit is pre-coated with 'Syntide-2' phosphorylated by CaMKII. The detector antibody (MS-6E6) is conjugated to horseradish peroxidase and specifically detects the phosphorylated form of 'Syntide-2'.

To perform the assay, the tested hits were first diluted with the kinase buffer provided with the kit. The hits' solutions were then pipetted into assay wells to yield final concentrations of 0.1, 1.0 and 10 μM and occasionally at 0.2 and 0.02 μM. Subsequently, CaMKII was added to each well as aqueous solution (0.01 units in 10 μL) and allowed to phosphorylate the bound substrate in the presence of CaCl$_2$, Calmodulin and ATP. The amount of phosphorylated substrate was measured by allowing it to bind with the detector antibody conjugated to horseradish peroxidase, which then catalyzes the conversion of the chromogenic substrate tetramethylbenzidine (TMB) from a colorless solution to a blue solution. The color is quantified by spectrophotometry and reflects the relative activity of CaMKII. Samples' absorbances were determined at a wavelength of 650 nm using a plate reader (Bio-Tek instruments ELx 800, USA). Inhibition of CaMKII was calculated as percent activity of the uninhibited CaMKII enzyme control. KN-62 was used as positive control (Table 6). Negative controls were prepared by adding the enzyme to the kinase reaction buffer only.[40]

Acknowledgments

Supplementary data

Supplementary data associated with this article can be found, in the online version, at doi:10.1016/j.bmc.2011.10.071.

References and notes

1. Hudmon, A.; Schulman, H. *Biochem. J.* **2002**, *364*, 593.
2. Hund, T.; Decker, K.; Kanter, E.; Mohler, P.; Boyden, P.; Schuessler, R.; Yamada, K.; Rudy, Y. *J. Mol. Cell. Cardiol.* **2008**, *45*, 420.
3. Anderson, M. *Pharmacol. Ther.* **2005**, *106*, 39.
4. Kurokawa, H.; Osawa, M.; Kurihara, H.; Katayama, N.; Tokumitsu, H.; Windells, M. S.; Kainosh, M.; Ikura, M. *J. Mol. Biol.* **2001**, *312*, 59.
5. Levy, D.; Wang, D.; Lu, Q.; Chen, Z.; Perumattam, J.; Xu, Y.; Liclican, A.; Higaki, J.; Dong, H.; Laney, M.; Mavunkel, B.; Dugar, S. *Bioorg. Med. Chem. Lett.* **2008**, *18*, 2390.
6. Levy, D.; Wang, D.; Lu, Q.; Chen, Z.; Perumattam, J.; Xu, Y.; Higaki, J.; Dong, H.; Liclican, A.; Laney, M.; Mavunkel, B.; Dugar, S. *Bioorg. Med. Chem. Lett.* **2008**, *18*, 2395.
7. Taha, M. O.; Bustanji, Y.; Al-Ghussein, M. A. S.; Mohammad, M.; Zalloum, H.; Al-Masri, I. M.; Atallah, N. *J. Med. Chem.* **2007**, *51*, 2062.
8. Taha, M. O.; Atallah, N.; Al-Bakri, A. G.; Paradis-Bleau, C.; Zalloum, H.; Younis, K.; Levesque, R. C. *Bioorg. Med. Chem.* **2008**, *16*, 1218.
9. Taha, M. O.; Bustanji, Y.; Al-Bakri, A. G.; Yousef, M.; Zalloum, W. A.; Al-Masri, I. M.; Atallah, N. *J. Mol. Graphics Modell.* **2007**, *25*, 870.
10. Al-masri, I. M.; Mohammad, M. K.; Taha, M. O. *Chem. Med. Chem.* **2008**, *3*, 1763.
11. Taha, M. O.; Dahabiyeh, L. A.; Bustanji, Y.; Zalloum, H.; Saleh, S. *J. Med. Chem.* **2008**, *51*, 6478.
12. Al-Nadaf, A.; Abu Sheikha, G.; Taha, M. O. *Bioorg. Med. Chem.* **2010**, *18*, 3088.
13. Abu-Hammad, A.; Zalloum, W. A.; Zalloum, H.; Abu-Sheikha, G.; Taha, M. O. *Eur. J. Med. Chem.* **2009**, *44*, 2583.
14. Abu Khalaf, R.; Abu Sheikha, G.; Bustanji, Y.; Taha, M. O. *Eur. J. Med. Chem.* **2010**, *45*, 1598.
15. Al-Sha'er, M. A.; Taha, M. O. *Eur. J. Med. Chem.* **2010**, *45*, 4316.
16. Al-Sha'er, M. A.; Taha, M. O. *J. Chem. Inform. Model.* **2010**, *50*, 1706.
17. Taha, M. O.; Trarairah, M.; Zalloum, H.; Abu Sheikha, G. *J. Mol. Graphics Modell.* **2010**, *28*, 383.
18. Abu Khalaf, R.; Abdula, A.; Mubarak, M.; Taha, M. O. *J. Mol. Model.* **2011**, *17*, 443.
19. Abdula, A.; Abu Khalaf, R.; Mubarak, M.; Taha, M. *J. Comput. Chem.* **2010**, *26*, 463.
20. Lu, Q.; Chen, Z.; Perumattam, J.; Wang, D.; Liang, W.; Xu, Y.; Do, S.; Bonaga, L.; Higaki, J.; Dong, H.; Liclican, A.; Sideris, S.; Laney, M.; Dugar, S.; Mavunkel, B.; Levy, D. *Bioorg. Med. Chem. Lett.* **2008**, *18*, 2399.
21. Mavunkel, B.; Xu, Y.; Goyal, B.; Lim, D.; Lu, Q.; Chen, Z.; Wang, D.; Higaki, J.; Chakraborty, I.; Liclican, A.; Sideris, S.; Laney, M.; Delling, U.; Catalano, R.; Higgins, L.; Wang, Y.; Wang, J.; Feng, Y.; Dugar, S.; Levy, D. *Bioorg. Med. Chem. Lett.* **2008**, *18*, 2404.
22. *CATALYST 4.11 Users' Manual*; Accelrys Software Inc.: San Diego, CA, 2005.
23. *Discovery Studio version 2.5 (DS 2.5) User Manual*; in, Accelrys Inc.: San Diego, CA, 2009.
24. Sheridan, R. P.; Kearsley, S. K. *Drug Discovery Today* **2002**, *7*, 903.
25. Li, H.; Sutter, J.; Hoffmann, R. In *Pharmacophore Perception, Development, and Use in Drug Design*; Güner, O. F., Ed.; International University Line: La Jolla, CA, 2000; p 173.
26. Sutter, J.; Güner, O.; Hoffmann, R.; Li, H.; Waldman, M. In *Pharmacophore Perception, Development, and Use in Drug Design*; Güner, O. F., Ed.; International University Line: La Jolla, CA, 2000; p 501.
27. Poptodorov, K.; Luu, T.; Langer, T.; Hoffmann, R. In *Methods and Principles in Medicinal Chemistry. Pharmacophores and Pharmacophores Searches*; Hoffmann, R. D., Ed.; Wiley-VCH: Weinheim, Germany, 2006; Vol. 2, pp 17–47.
28. Kurogi, Y.; Guner, O. F. *Curr. Med. Chem.* **2001**, *8*, 1035.
29. Bersuker, I. B.; Bahçeci, S.; Boggs, J. E. In *Pharmacophore Perception, Development, and Use in Drug Design*; Güner, O. F., Ed.; International University Line: La Jolla, CA, 2000; p 457.
30. Fisher, R. *The Principle of Experimentation Illustrated by a Psycho-Physical*, 8th ed.; ExpeHafner Publishing Co., Hafner Publishing: New York, 1966.
31. *CERIUS2, QSAR Users' Manual, version 4.10*; Accelrys Inc.: San Diego, CA, 2005, pp 43–88, 221–235, 237–250.
32. Ramsey, L. F.; Schafer, W. D. *The Statistical Sleuth*, 1st ed.; Wadsworth Publishing Company: Belmont, CA, 1997.
33. Clement, O. O.; Mehl, A. T. In *Pharmacophore Perception, Development, and Use in Drug Design*; Guner, O. F., Ed.; International University Line: La Jolla, CA, 2000; p 71.
34. Verdonk, M. L.; Marcel, L.; Berdini, V.; Hartshorn, M. J.; Mooij, W. T. M.; Murray, C. W.; Taylor, R. D.; Watson, P. *J. Chem. Inform. Comput. Sci.* **2004**, *44*, 793.
35. Zweig, M. H.; Campbell, G. *Clin. Chem.* **1993**, *39*, 561.
36. Kirchmair, J.; Markt, P.; Distinto, S.; Wolber, G.; Langer, T. *J. Comput. Aided Mol. Des.* **2008**, *22*, 213.
37. Irwin, J. J.; Shoichet, B. K. *J. Chem. Inf. Comput. Sci.* **2005**, *45*, 177.
38. Triballeau, N.; Acher, F.; Brabet, I.; Pin, J.-P.; Bertrand, H.-O. *J. Med. Chem.* **2005**, *48*, 2534.
39. Lipinski, C. A.; Lombardo, F.; Dominy, B. W.; Feeney, P. J. *Adv. Drug Delivery Rev.* **2001**, *46*, 3.
40. Veber, D. F.; Johnson, S. R.; Cheng, H. Y.; Smith, B. R.; Ward, K. W.; Kopple, K. D. *Bioorg. Med. Chem.* **2002**, *45*, 2615.
41. *CycLex, CaM kinase II Assay Kit (Cat# CY-1173) Users' Manual*; CycLex Co., Ltd: Ina, Nagano, Japan, 2009.
42. Davies, S.; Reddy, H.; Caivano, M.; Cohen, P. *Biochem. J.* **2000**, *351*, 95.
43. Mirzoeva, S.; Koppal, T.; Petrova, T.; Lukas, T.; Watterson, D.; Van Eldik, L. *Brain Res.* **1999**, *844*, 126.
44. Krovat, E. M.; Langer, T. *J. Med. Chem.* **2003**, *46*, 716.
45. Davies, S.; Reddy, H.; Caivan, M.; Cohen, P. *Biochem. J.* **2000**, *351*, 95.
46. Leftheris, K.; Ahmed, G.; Chan, R.; Dyckman, A.; Hussain, Z.; Ho, K.; Hynes, J.; Letourneau, J.; Li, W.; Lin, S.; Metzger, A.; Moriarty, K.; Riviello, C.; Shimshock, Y.; Wen, J.; Wityak, J.; Wrobleski, S.; Wu, H.; Wu, J.; Desai, M.; Gillooly, K.; Lin, T.; Loo, D.; McIntyre, K.; Pitt, S.; Shen, D.; Shuster, R.; Zhang, D.; Diller, A.; Doweyko, T.; Sack, J.; Baldwin, J.; Barrish, J.; Dodd, J.; Henderson, I.; Kanner, S.; Schieven, G.; Webb, M. *J. Med. Chem.* **2004**, *47*, 6283.
47. Sossalla, S.; Fluschnik, N.; Schotola, H.; Ort, K.; Neef, S.; Schulte, T.; Wittkoepper, K.; Renner, A.; Schmitto, J.; Gummert, J. *Circ. Res.* **2010**, *107*, 1150.
48. Stolen, T.; Hoydal, M.; Kemi, O.; Catalucci, D.; Ceci, M.; Aasum, E.; Larsen, T.; Rolim, N.; Condorelli, G.; Smith, G. *Circ. Res.* **2009**, *105*, 527.
49. MacDonnell, S.; Weisser-Thomas, J.; Kubo, H.; Hanscome, M.; Liu, Q.; Jaleel, N.; Berretta, R.; Chen, X.; Brown, J.; Sabri, A. *Circ. Res.* **2009**, *105*, 316.
50. Kohlhaas, M.; Zhang, T.; Seidler, T.; Zibrova, D.; Dybkova, N.; Steen, A.; Wagner, S.; Chen, L.; Heller Brown, J.; Bers, D. *Circ. Res.* **2006**, *98*, 235.
51. Desai, R. M. *Indian J. Chem.* **2004**, *105*, 367.
52. Fontana, P.; Amorosa, M.; Alfieri, L. *Pubbl. univ. cattolica S. Cuore* **1960**, *77*, 115.
53. Curd, S.; Landquist, K.; Rose, L. *J. Chem. Soc.* **1947**, *154*, 154.
54. Desai, P. S.; Desai, K. R. *Indian J. Chem.* **1990**, 688.
55. Wolf, N.; Schuldt, H.; Baldwin, M. *Science* **1955**, *121*, 61.
56. Fahnenstich, R.; Schwarze, W.; Bertram, H.; Tanner, H. Ger. Offen. Patent No.: DE 2311237, 1974, 13.
57. Skoog, D. A.; West, D. M.; Holler, F. J. *Fundamentals of Analytical Chemistry*, 7th ed.; Thomson Learning, Inc.: USA, 1996.